

Energy levels and magneto-optical transitions in parabolic quantum dots with spin-orbit coupling

Pekka Pietiläinen*[†] and Tapash Chakraborty*[‡]

**Department of Physics and Astronomy, University of Manitoba, Winnipeg, Canada R3T 2N2 and*

[†]*Department of Physical Sciences/Theoretical Physics,
P.O. Box 3000, FIN-90014 University of Oulu, Finland*

(Dated: November 8, 2018)

We report on the electronic properties of few interacting electrons confined in a parabolic quantum dot based on a theoretical approach developed to investigate the influence of Bychkov-Rashba spin-orbit (SO) interaction on such a system. We note that the spin-orbit coupling profoundly influences the energy spectrum of interacting electrons in a quantum dot. Here we present accurate results for the energy levels and optical-absorption spectra for parabolic quantum dots containing upto four interacting electrons, in the presence of spin-orbit coupling and under the influence of an externally applied, perpendicular magnetic field. We have described in detail about a very accurate numerical scheme to evaluate these quantities. We have evaluated the effects of SO coupling on the Fock-Darwin spectra for quantum dots made out of three different semiconductor systems, InAs, InSb, and GaAs. The SO coupling on the single-electron spectra manifests itself by primarily lifting of the degeneracy at zero magnetic field, rearrangement of some of the energy levels at small magnetic fields, and level repulsions at high fields. These are explained as due to mixing of different spinor states for increasing strength of SO coupling. As a consequence, the corresponding absorption spectra reveal anticrossing structures in the two main lines of the spectra. For the interacting many-electron systems we observed the appearance of discontinuities, anticrossings, and new modes that appear in conjunction with the two main absorption lines. These additional features arise entirely due to the SO coupling and are a consequence of level crossings and level repulsions in the energy spectra. An intricate interplay between the SO coupling and the Zeeman energies are shown to be responsible for these new features seen in the energy spectra. Optical absorption spectra for all three types of quantum dots studied here show a common feature: new modes appear, mostly near the upper main branch of the spectra around 2 tesla that become stronger with increasing SO coupling strength. Among the three types of systems considered here, optical signatures of the SO interaction is found to be the strongest in the absorption spectra of the GaAs quantum dot, but only at very large values of the SO coupling strength, and appears to be the weakest for the InSb quantum dot. Experimental observation of these new modes that appear solely due to the presence of SO coupling would provide a rare glimpse on the role of SO coupling in nanostructured quantum systems.

PACS numbers: 71.70.Ej, 72.25.Dc, 72.25.-b

I. INTRODUCTION

Impressive developments in nanofabrication technology have made it now possible to design the quantum dots and coupled quantum dots at the nanoscale. These systems comprise of a few electrons that are quantum confined, for our present purpose, at the semiconductor interface to form the zero-dimensional systems. What is more remarkable is that the electronic states in these systems can be precisely controlled via the external voltages [1]. Magneto-optical studies of parabolic quantum dots (described as *artificial atoms* [2] by us in 1990) have been intensely explored for more than a decade [2, 3, 4, 5, 6] in order to understand its unique electronic and optical properties and as promising candidates for optoelectronic devices, applications in optical quantum information technology, etc. [7, 8]. As a result of these studies, a very good theoretical and experimental understanding of the single-electron states in the dot has already been achieved. At the most basic level, the solution of the Schrödinger equation for an electron confined by a har-

monic potential, $v_c = \frac{1}{2}m^*\omega_0 r^2$, ω_0 is the confinement potential strength, in the presence of an external perpendicular magnetic field is well known since the beginning of quantum mechanics [4, 9]. The eigenvalues in this case are given by

$$E_{nl} = (2n + |l| + 1) \hbar\Omega - \frac{1}{2}l\hbar\omega_c$$

where $n = 0, 1, 2, \dots$ and $l = 0, \pm 1, \dots$, are the principal and azimuthal quantum numbers respectively, $\Omega^2 = [\omega_0^2 + \frac{1}{4}\omega_c^2]$, and ω_c is the cyclotron frequency. Dipole-allowed transitions among these energy levels will have energies [2, 4, 5]

$$\Delta E_{\pm} = \hbar\Omega \pm \frac{1}{2}\hbar\omega_c.$$

This relation has been verified to great accuracy by a variety of experiments [3, 4, 6]. Interestingly, however, the observed magnetic field dependent FIR absorption in quantum dots containing more than one electron was found to be essentially *independent* of the number of electrons confined and instead was dominated by the above

relation for ΔE_{\pm} [5]. It was a rather puzzling result because according to this, magneto-optics was clearly incapable of providing any relevant information about the effect of mutual interactions of the confined electrons. The puzzle was later resolved by Maksym and Chakraborty [2, 3, 4, 10], who pointed out that for a parabolic QD in an external magnetic field, the dipole interaction is a function of the center-of-mass (CM) coordinate alone and the inter-electron interaction does not play any role. Despite this somewhat disappointing performance of a parabolic dot, FIR spectroscopy of QDs (parabolic or otherwise) has generated enormous interest for over a decade that is yet to subside [6]. In this paper we include another interesting element into the problem, the spin-orbit (SO) interaction. We demonstrate here that in the presence of spin-orbit coupling the magneto-optical transitions show many new and interesting features that can be tuned by the SO coupling. Based on these results, we propose that magneto-optical transitions are best suited to determine optically the unique effect of SO coupling in quantum dots described below [11].

Interest on the role of the spin-orbit coupling in nanostructured systems is now at its peak, due largely to its relevance to spin transport in low-dimensional electron channels [12, 13]. The intriguing possibility of tuning the SO field and thereby coherently manipulate electron spins in quantum dots has sparked major activities in the past years [14, 15, 16, 17, 18, 19, 20, 21, 22, 23, 24, 25, 26, 27, 28, 29, 30, 31]. It is hoped that an improved understanding of spin dynamics in the QDs might pave the way for future electronic and information processing, especially in quantum computing and quantum communication [32]. Spin degree of freedom is perhaps more advantageous than charge because unlike charge, spin is not coupled to electromagnetic noise and therefore have much longer coherence time [33]. Improved knowledge of the influence of spin-orbit coupling in quantum dots is therefore quite essential in this pursuit. While the majority of experimental efforts has focused on magneto-transport measurements [34], here we present the results for the optical absorption spectra that are experimentally observable and could, in principle, provide an important probe of SO coupling in few-electron quantum dots.

The spin-orbit interaction in semiconductor heterostructures can be caused by an electric field perpendicular to the two-dimensional electron gas (2DEG). Riding on an electron, this electric field will be *felt* as an effective magnetic field lying in the plane of the 2DEG, perpendicular to the wave vector k of the electron. The effective Zeeman interaction of the electron spin with the field lifts the spin degeneracy (internal Zeeman effect). This is usually referred to in the literature as the Bychkov-Rashba mechanism. This results in an isotropic spin splitting energy Δ_{SO} at $B = 0$ proportional to k [35].

Let us consider an electron in the 2DEG moving with a velocity \vec{v} in the presence of an electric field \vec{E} . In the rest frame of the electron, this transforms (relativistically)

into an effective magnetic field \vec{B}_{eff} ,

$$\vec{B}_{\text{eff}} = -\frac{1}{2c^2}\vec{v} \times \vec{E}$$

where c is the speed of light. The magnetic moment of the electron will then couple to \vec{B}_{eff} . The resulting spin-orbit interaction is,

$$\begin{aligned} \mathcal{H}_{\text{SO}} &= \vec{\mu} \cdot \vec{B}_{\text{eff}} \\ &= -\frac{1}{2c^2}\vec{\mu} \cdot (\vec{v} \times \vec{E}) = \frac{e\hbar^2}{4m_0^2c^2}\vec{\sigma} \cdot (\vec{k} \times \vec{E}) \end{aligned}$$

since, $\vec{\mu} = -\frac{e\hbar}{2m_0}\vec{\sigma}$, and $\vec{v} = \hbar\vec{k}/m_0$. It can be rewritten as

$$\mathcal{H}_{\text{SO}} = \frac{e\hbar^2}{4m_0^2c^2}\vec{\sigma} \cdot (\vec{k} \times \vec{E}) = \alpha' \langle E_z \rangle (-i\vec{\nabla} \times \vec{\sigma})_z, \quad (1)$$

where the electric field is aligned along the z axis.

Alternatively, a general spin-orbit Hamiltonian that stems directly from the quadratic in v/c expansion of the Dirac equation is [36]

$$\mathcal{H}_{\text{SO}} = \frac{e\hbar}{(2m_0c)^2}\vec{\nabla}V(\vec{r}) \cdot (\vec{\sigma} \times \vec{p}). \quad (2)$$

The electric field associated with $V(\vec{r})$ is $\vec{E}(\vec{r}) = \vec{\nabla}V(\vec{r})$, and is directed along the z direction. The spin-orbit interaction Hamiltonian

$$\begin{aligned} \mathcal{H}_{\text{SO}} &= \frac{e\hbar^2}{(2m_0c)^2}\langle E_z \rangle \frac{1}{\hbar}(\vec{\sigma} \times \vec{p}) \cdot \hat{n} = \alpha' \langle E_z \rangle \frac{1}{\hbar}(\vec{\sigma} \times \vec{p}) \cdot \hat{n} \\ &= \alpha' \langle E_z \rangle (\vec{\sigma} \times \vec{k}) \cdot \hat{n}, \end{aligned}$$

where $\alpha' = e(\hbar/2m_0c)^2$ is then identical to that in Eq. (1). An important point to note here is that a non-vanishing gradient in Eq. (2) requires that the system must have inversion asymmetry. In the present case that arises from the structural inversion asymmetry [37]. The spin-orbit interaction that we are here concerned with is therefore described by the Hamiltonian

$$\mathcal{H}_{\text{SO}} = \alpha(\vec{k} \times \vec{\sigma})_z = i\alpha \left(\sigma_y \frac{\partial}{\partial x} - \sigma_x \frac{\partial}{\partial y} \right), \quad (3)$$

where the z axis is chosen perpendicular to the 2DEG (in the xy -plane), α is the spin-orbit coupling constant, which is sample dependent and is proportional to the interface electric field that confines the electrons in the $x - y$ plane, $\vec{\sigma} = (\sigma_x, \sigma_y, \sigma_z)$ denotes the Pauli matrices, and \vec{k} is the planar wave vector. This is the Bychkov-Rashba Hamiltonian [35] that has been receiving of late rather widespread attention [34].

The single-electron Hamiltonian for the 2DEG including the Bychkov-Rashba term has the form

$$\begin{aligned}\mathcal{H} &= \frac{\vec{p}^2}{2m^*} + \frac{\alpha}{\hbar} (\vec{\sigma} \times \vec{p})_z \\ &= -\frac{\hbar^2}{2m^*} \vec{\nabla}^2 + i\alpha \left(\sigma_y \frac{\partial}{\partial x} - \sigma_x \frac{\partial}{\partial y} \right) \\ &= \begin{pmatrix} -\frac{\hbar^2}{2m^*} \vec{\nabla}^2 & \alpha \nabla^- \\ -\alpha \nabla^+ & -\frac{\hbar^2}{2m^*} \vec{\nabla}^2 \end{pmatrix}\end{aligned}$$

where $\vec{\nabla}^2 = \partial^2/\partial x^2 + \partial^2/\partial y^2$ and $\nabla^\pm = \partial/\partial x \pm i\partial/\partial y$.

Since the operators \hat{p}_x and \hat{p}_y commute with the Hamiltonian, we can search for $\alpha \neq 0$ eigenstates of the form

$$\Psi(k_x, k_y) = e^{ik_x x + ik_y y} \sum_{\sigma} C^{\sigma} |\sigma\rangle = e^{ik_x x + ik_y y} \begin{pmatrix} C^+ \\ C^- \end{pmatrix},$$

with $|\sigma\rangle = \begin{pmatrix} 1 \\ 0 \end{pmatrix}$ (spin up) or $\begin{pmatrix} 0 \\ 1 \end{pmatrix}$ (spin down). Solutions of

$$\mathcal{H}\Psi(k_x, k_y) = \mathcal{E}\Psi(k_x, k_y)$$

are readily obtained as

$$\Psi^{\pm}(k_x, k_y) = \frac{1}{\sqrt{2}} \begin{pmatrix} 1 \\ \frac{\pm k_y \mp ik_x}{k} \end{pmatrix} e^{ik_x x + ik_y y}.$$

The energy dispersion then consists of two branches

$$\mathcal{E}^{\pm}(k) = \frac{\hbar^2}{2m^*} k^2 \pm \alpha k$$

with an energy separation $\Delta_{\text{SO}} = \mathcal{E}^+ - \mathcal{E}^- = 2\alpha k$ for a given k . The spin parts of the wave functions $\chi^{\pm}(k_x, k_y)$ are mutually orthogonal and $\langle \chi^{\pm} | \sigma_z | \chi^{\pm} \rangle = 0$. Therefore in the states Ψ^{\pm} the spins of the electrons lie in the xy -plane and point in opposite directions. In addition,

$$\langle \chi^{\pm} | \sigma_x | \chi^{\pm} \rangle = \frac{2k_y}{k}, \quad \langle \chi^{\pm} | \sigma_y | \chi^{\pm} \rangle = -\frac{2k_x}{k},$$

i.e., the spins are *perpendicular* to the momentum (k_x, k_y) . Spatial alignment of spins therefore depends on the wave vector [12, 35]. The Fermi surface is a pair of concentric circles with radii $k_{F,max}$ and $k_{F,min}$. In the present paper, we are dealing with systems having rotational symmetry. The formalism in that case is derived in detail in Sect. II.

Several experimental groups [34] investigating the Shubnikov-de Haas (SdH) oscillations in a 2DEG confined at the heterojunctions with a narrow-gap quantum well (e.g., InGaAs/InAlAs, InAs/GaSb, etc.) have already established that lifting of spin degeneracy results from inversion asymmetry of the structure which invokes

an electric field perpendicular to the layer. Experimentally observed values of the SO coupling strength α lie in the range of 5 – 45 meV.nm [34]. Energy levels of two interacting electrons confined in a parabolic quantum dot in an external magnetic field were recently reported by us for this range of SO coupling strength [31]. In the absence of SO coupling, electron-electron interaction causes the ground state energy to jump from one angular momentum value to another as the magnetic field is increased [2, 4]. The influence of the SO coupling is primarily to move the energy level crossings to weaker fields [31].

Our paper is organized as follows: In Sect. II, we present the essential formalism for our study of non-interacting electrons in parabolic QDs in the presence of spin-orbit interaction. The single-electron basis and the dipole matrix elements are derived here. We also explain why the dipole-allowed transitions are so significantly influenced by the presence or absence of the SO interaction. The classic Fock-Darwin spectra for three different quantum dots systems (InAs, InSb, and GaAs) with or without the SO coupling are presented and discussed in detail. The formalism for the many-electron system in a parabolic QD with SO coupling is presented in Sect. III. The complexities of introducing the SO coupling, in particular for interacting electrons, are made clear in Sect. III. The task of finding a suitable numerical technique is even more challenging, and an approach that is appropriate for our purpose is described in the Appendix. Numerical results for the energy levels and the optical absorption spectra for the three types of QDs containing upto four interacting electrons are presented and discussed in Sect. IV. It should be pointed out that the low-lying energy levels calculated here for the single- and multi-electron quantum dots can, in principle, be observed in transport [38], or capacitance spectroscopy [39]. Given the acute interest on the influence of SO coupling in nanostructured systems and the resulting intense activities on this topic, it is no surprise that many different theoretical techniques have been put forward in the literature. To view our work in proper perspective, we present a brief review of many of those theoretical papers in Sect. V. We conclude with a brief outlook for future work along this direction in Sect. VI. For a brief account of our earlier work on SO coupling effects in parabolic QDs, see Refs. [11, 31].

II. SINGLE-ELECTRON PICTURE

The Hamiltonian for an electron in a parabolic confinement and under external magnetic field is given by

$$\begin{aligned}\mathcal{H}_0 &= \frac{1}{2m^*} \left(\vec{p} - \frac{e}{c} \vec{A} \right)^2 + \frac{1}{2} m^* \omega_0^2 r^2 \\ &+ \frac{\alpha}{\hbar} \left[\vec{\sigma} \times \left(\vec{p} - \frac{e}{c} \vec{A} \right) \right]_z + \frac{1}{2} g \mu_B B \sigma_z.\end{aligned}\quad (4)$$

Here $\vec{\sigma}$ is the vector of Pauli matrices, i.e.

$$\begin{aligned}\vec{\sigma} &= \sigma_x \vec{i} + \sigma_y \vec{j} + \sigma_z \vec{k} \\ &= \begin{pmatrix} 0 & 1 \\ 1 & 0 \end{pmatrix} \vec{i} + \begin{pmatrix} 0 & -i \\ i & 0 \end{pmatrix} \vec{j} + \begin{pmatrix} 1 & 0 \\ 0 & -1 \end{pmatrix} \vec{k}. \quad (5)\end{aligned}$$

We work in the symmetric gauge and the vector potential corresponding to the external perpendicular magnetic field is

$$\vec{A} = \frac{B}{2}(-y, x, 0). \quad (6)$$

The term $\frac{\alpha}{\hbar} \left[\vec{\sigma} \times \left(\vec{p} - \frac{e}{c} \vec{A} \right) \right]_z$ in the Hamiltonian is the spin-orbit (SO) coupling due to the inhomogenous potential confining the electrons to the 2D plane and possible external gate voltages applied on the top of the dot. The parameter α determines the strength of this coupling and, in case of external gate voltages its magnitude can be varied. Finally, the last term $\frac{1}{2} g \mu_B B \sigma_z$ is the ordinary Zeeman coupling g being the effective Lande' g -factor.

The eigenstates of the single particle problem

$$\mathcal{H}_0 \phi = \varepsilon \phi \quad (7)$$

are clearly two-component spinors

$$|\lambda\rangle = \begin{pmatrix} \phi^\uparrow \\ \phi^\downarrow \end{pmatrix}. \quad (8)$$

Writing the equation (7) in polar coordinates and substituting a trial wave function of the form

$$\phi = \begin{pmatrix} f^\uparrow(r) e^{i\ell^\uparrow \theta} \\ f^\downarrow(r) e^{i\ell^\downarrow \theta} \end{pmatrix} \quad (9)$$

it is easy to see that the quantum numbers ℓ^\uparrow and ℓ^\downarrow must be integers and that they depend on each other in the way

$$\ell^\uparrow = \ell^\downarrow - 1. \quad (10)$$

Hence we need only one quantum number for the angular motion, i.e. solutions of the single particle equation (7) are of the form

$$|\lambda\rangle = |k, \ell\rangle = \begin{pmatrix} f_{k,\ell}^\uparrow(r) e^{i\ell\theta} \\ f_{k,\ell}^\downarrow(r) e^{i(\ell+1)\theta} \end{pmatrix}. \quad (11)$$

Here the quantum number k is associated with radial motion (and not to be confused with the wave vector described in Sect.I). The form of the spinor (11) simply restates the fact that under SO coupling the good quantum numbers are related to $\vec{L} + \vec{S}$. In our case the conserved quantity is

$$j = \ell^{\uparrow,\downarrow} + s_z^{\uparrow,\downarrow} = \ell + \frac{1}{2} \quad (12)$$

where $s_z = \pm \frac{1}{2}$ depending on the component of the spinor, i.e., $+\frac{1}{2}$ for the upper component and $-\frac{1}{2}$ for the lower one.

In order to find the radial wavefunctions $f^{\uparrow,\downarrow}$ we transform to dimensionless units by setting

$$\begin{aligned}\omega_c &= \frac{eB}{m^*c}, \quad a^2 = \frac{\hbar}{m^*\omega_0 (1 + \omega_c^2/4\omega_0^2)^{\frac{1}{2}}}, \\ x &= \frac{r^2}{a^2}, \quad \beta = \frac{m^*\alpha a}{\hbar^2}, \\ b_R &= \frac{ea^2B}{\hbar^2}, \quad \eta^\pm = 1 \pm 2b_R, \\ \nu_\ell^{\uparrow,\downarrow} &= \frac{\ell\omega_c}{4\omega_0 (1 + \omega_c^2/4\omega_0^2)^{\frac{1}{2}}} \pm \frac{g\mu_B B}{4\hbar\omega_0 (1 + \omega_c^2/4\omega_0^2)^{\frac{1}{2}}}, \\ \varepsilon &= 2\hbar\omega_0 \left(1 + \frac{\omega_c^2}{4\omega_0^2} \right)^{\frac{1}{2}} \nu, g^{\uparrow,\downarrow}(x) = f^{\uparrow,\downarrow}(r).\end{aligned}$$

Substituting these into the Hamiltonian (4) the radial part of the equation (7) takes the form

$$\begin{aligned}xg^{\uparrow''} + g^{\uparrow'} + \left(\nu - \frac{\ell^2}{4x} - \frac{x}{4} + \nu_\ell^\uparrow \right) g^\uparrow \\ - \beta x^{1/2} \left(g^{\downarrow'} + \frac{\ell+1}{2x} g^\downarrow + b_R g^\downarrow \right) = 0 \quad (13)\end{aligned}$$

$$\begin{aligned}xg^{\downarrow''} + g^{\downarrow'} + \left(\nu - \frac{(\ell+1)^2}{4x} - \frac{x}{4} + \nu_{\ell+1}^\uparrow \right) g^\downarrow \\ + \beta x^{1/2} \left(g^{\uparrow'} - \frac{\ell}{2x} g^\uparrow - b_R g^\uparrow \right) = 0 \quad (14)\end{aligned}$$

of two coupled differential equations. For $\beta = 0$ (i.e., $\alpha = 0$) these equations describe radial motions of two independent two-dimensional harmonic oscillators with eigenvalues

$$\nu_{n\ell}^{\uparrow,\downarrow} = n + \frac{|\ell| + 1}{2} + \nu_\ell^{\uparrow,\downarrow} \quad (15)$$

and the eigenfunctions

$$g_{n\ell} = \sqrt{\frac{n!}{(n+|\ell|)!}} e^{-x/2} x^{|\ell|/2} L_n^{|\ell|}(x). \quad (16)$$

Here $L_n^{|\ell|}$ is the associated Laguerre polynomial defined, for example, by the formula

$$L_n^{|\ell|}(x) = e^x x^{-|\ell|} \frac{d^n}{dx^n} \left(e^{-x} x^{n+|\ell|} \right).$$

Therefore it is logical to seek the solution for Eqs. (13, 14) in the form of the expansion [14]

$$g^{\uparrow,\downarrow} = \sum_{n=0} c_{n,\ell}^{\uparrow,\downarrow} g_{n,\ell}. \quad (17)$$

In spinor language (9) this corresponds to the expan-

sion

$$\begin{aligned}
|\lambda\rangle &= \begin{pmatrix} \sum_{n=0} c_{n,\ell}^\uparrow g_{n,\ell}(x) e^{i\ell\theta} \\ \sum_{n=0} c_{n,\ell+1}^\downarrow g_{n,\ell+1}(x) e^{i(\ell+1)\theta} \end{pmatrix} \\
&= e^{i\ell\theta} \sum_{n=0} c_{n,\ell}^\uparrow \begin{pmatrix} g_{n,\ell}(x) \\ 0 \end{pmatrix} + \\
&\quad e^{i(\ell+1)\theta} \sum_{n=0} c_{n,\ell+1}^\downarrow \begin{pmatrix} 0 \\ g_{n,\ell+1}(x) \end{pmatrix}. \quad (18)
\end{aligned}$$

The coefficients $c_{n,\ell}^{\uparrow,\downarrow}$ can be obtained by minimizing the expectation value $\langle \lambda | \mathcal{H}_0 | \lambda \rangle$. At this point it is useful to relabel our spinors. For example, for non-negative values of ℓ we set

$$u_{2n} = e^{i\ell\theta} \begin{pmatrix} g_{n,\ell}(x) \\ 0 \end{pmatrix} \quad (19)$$

$$u_{2n+1} = e^{i(\ell+1)\theta} \begin{pmatrix} 0 \\ g_{n,\ell+1}(x) \end{pmatrix} \quad (20)$$

$$z_{2n} = c_{n,\ell}^\uparrow \quad (21)$$

$$z_{2n+1} = c_{n,\ell+1}^\downarrow. \quad (22)$$

The minimization of

$$\langle \lambda | \mathcal{H}_0 | \lambda \rangle = \sum_{n,n'} z_{n'} z_n \langle u_{n'} | \mathcal{H}_0 | u_n \rangle$$

leads now to the diagonalization of the symmetric tridiagonal matrix \mathcal{H} with diagonal

$$\text{diag } \mathcal{H} = (\nu_{0,\ell}^\uparrow, \nu_{0,\ell+1}^\downarrow, \dots, \nu_{n,\ell}^\uparrow, \nu_{n,\ell+1}^\downarrow, \dots) \quad (23)$$

and subdiagonal

$$\text{subdiag } \mathcal{H} = \frac{\beta}{2} \left(0, \sqrt{\ell+1} \eta^+, \eta^-, \dots, \sqrt{n} \eta^-, \sqrt{n+\ell+1} \eta^+, \sqrt{n+1} \eta^-, \dots \right). \quad (24)$$

The diagonalization yields a set of solutions: the set $\{\nu^{(k,\ell)}\}$ of eigenvalues and the set $\{z_n^{(k,\ell)}\}$ of eigenvectors indexed by the particular solution k and the fixed angular momentum ℓ . These are the energies of the spinors and the expansion coefficients (21,22). For negative values of ℓ the tridiagonal matrix consists of the diagonal

$$\text{diag } \mathcal{H} = (\nu_{0,\ell+1}^\downarrow, \nu_{0,\ell}^\uparrow, \dots, \nu_{n,\ell+1}^\downarrow, \nu_{n,\ell}^\uparrow, \dots) \quad (25)$$

and the subdiagonal

$$\text{subdiag } \mathcal{H} = -\frac{\beta}{2} (0, \sqrt{|\ell|} \eta^-, \eta^+, \dots, \sqrt{n} \eta^+, \sqrt{n+|\ell|} \eta^-, \sqrt{n+1} \eta^+, \dots). \quad (26)$$

The spinors thus obtained comprise our single-particle basis

$$\begin{aligned}
\mathcal{B}_S &= \{ |\lambda_i\rangle \mid i = 0, 1, 2, \dots \} \\
&= \{ |k, \ell\rangle \mid k = 0, 1, 2, \dots; \ell = 0, \pm 1, \pm 2, \dots \}. \quad (27)
\end{aligned}$$

A. Dipole matrix elements

According to the Fermi golden rule the intensity of absorption in dipole approximation is proportional to the square of the matrix element

$$I = \langle f | \sum_{i=1}^N r_i e^{\pm i\theta_i} | i \rangle$$

when the transition goes from the initial N -particle state $|i\rangle$ to the final state $|f\rangle$. To evaluate this we need to know the dipole matrix elements $d_{\lambda',\lambda}$ between the spinor states $|\lambda'\rangle$ and $|\lambda\rangle$, i.e. the elements

$$d_{\lambda',\lambda} = \langle \lambda' | r e^{\pm i\theta} | \lambda \rangle = \langle k', \ell' | r e^{\pm i\theta} | k, \ell \rangle. \quad (28)$$

For simplicity we consider only the circular polarization $e^{+i\theta}$ (the other circular polarization is obtained by reversing the roles of λ and λ'). Substituting expansions (17) into the above expression (28) we get

$$\begin{aligned}
d_{\lambda',\lambda} &= a \delta_{\ell',\ell+1} \sum_n \left[c_n^\uparrow c_n^\uparrow \sqrt{n+\ell+1} - c_{n-1}^\uparrow c_n^\uparrow \sqrt{n} \right. \\
&\quad \left. + c_n^\downarrow c_n^\downarrow \sqrt{n+\ell+2} - c_{n-1}^\downarrow c_n^\downarrow \sqrt{n} \right] \quad (29)
\end{aligned}$$

when $\ell \geq 0$,

$$\begin{aligned}
d_{\lambda',\lambda} &= a \delta_{\ell',0} \sum_n \left[c_n^\uparrow c_n^\uparrow \sqrt{n+1} - c_{n+1}^\uparrow c_n^\uparrow \sqrt{n+1} \right. \\
&\quad \left. + c_n^\downarrow c_n^\downarrow \sqrt{n+1} - c_{n-1}^\downarrow c_n^\downarrow \sqrt{n} \right] \quad (30)
\end{aligned}$$

when $\ell = -1$ and

$$\begin{aligned}
d_{\lambda',\lambda} &= a \delta_{\ell',\ell+1} \sum_n \left[c_n^\uparrow c_n^\uparrow \sqrt{n-\ell} - c_{n+1}^\uparrow c_n^\uparrow \sqrt{n+1} \right. \\
&\quad \left. + c_n^\downarrow c_n^\downarrow \sqrt{n-\ell-1} - c_{n+1}^\downarrow c_n^\downarrow \sqrt{n+1} \right] \quad (31)
\end{aligned}$$

when $\ell < -1$. The intensity is then obtained from $\mathcal{I} \propto |d_{\lambda_1 \lambda_2}|^2$ [40]. In all our figures for the absorption spectra, the size of the points is proportional to the calculated intensity.

The reason why dipole-allowed transitions in a parabolically confined quantum dot can be very different in the presence of SO interaction is explained as follows. When subjected to the radiation field with amplitude a and polarization \vec{e} , the vector potential \vec{A} in the single particle Hamiltonian

$$\begin{aligned}
\mathcal{H}_0 &= \frac{1}{2m^*} \left(\vec{p} - \frac{e}{c} \vec{A} \right)^2 + \frac{1}{2} m^* \omega_0^2 r^2 \\
&\quad + \frac{\alpha}{\hbar} \left[\vec{\sigma} \times \left(\vec{p} - \frac{e}{c} \vec{A} \right) \right]_z + \frac{1}{2} g \mu_B B \sigma_z
\end{aligned}$$

must be replaced with the potential

$$\vec{A} \rightarrow \vec{A} + \vec{A}_\omega, \quad \vec{A}_\omega = \vec{e} a e^{i\vec{k} \cdot \vec{r} - i\omega t}.$$

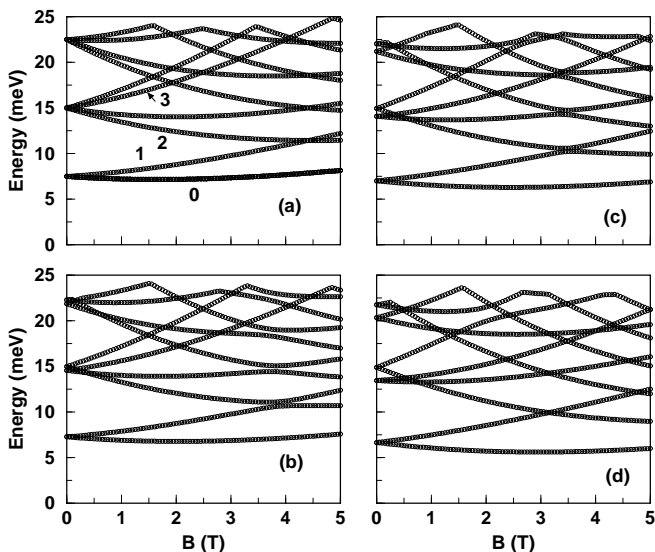


FIG. 1: Some of the low-lying energy states for non-interacting electrons confined in a InAs quantum dot for various values the SO coupling strength (in meV.nm), $\alpha = 0$ [a], $\alpha = 20$ [b], $\alpha = 30$ [c], and $\alpha = 40$ [d]. The labels in (a) are explained in the text.

In the dipole approximation we assume that

$$A_\omega \approx \vec{\epsilon} a e^{-i\omega t}$$

and correspondingly the Hamiltonian will be [41]

$$\mathcal{H} \approx \mathcal{H}_0 - \mathcal{H}' e^{-i\omega t},$$

where

$$\mathcal{H}' = \frac{ea}{m^*c} \vec{\epsilon} \cdot \left(\vec{p} - \frac{e}{c} \vec{A} \right) + \frac{\alpha ea}{\hbar c} [\vec{\sigma} \times \vec{\epsilon}]_z.$$

In a many-body system when $\alpha = 0$ the first term generates the CM density excitations where mutual interactions play no role. Consequently (in dipole approximation) only transitions between these modes are possible. When α is different from zero, the second term ($\propto \sigma_x \epsilon_y - \sigma_y \epsilon_x$) in \mathcal{H}' can create spin-density oscillations and interactions have effect on their properties. It is to be noted that, in SO coupled systems the dipole operator still retains its familiar form, $\hat{Q} = \frac{ea}{c} \vec{\epsilon} \cdot \vec{r}$, as is easily verified by evaluating its commutator with the Hamiltonian \mathcal{H}_0

$$[\hat{Q}, \mathcal{H}_0] = i\hbar \mathcal{H}'.$$

Dipole operator is independent of the electron spin. The dipole-allowed optical transitions are always between the same spin states, but the angular momenta must differ by unity. In the presence of SO coupling, neither the dipole operator nor the selection rule changes, but the SO interaction mixes the neighboring angular momentum values (l and $l + 1$) as well as the spin and hence the selection

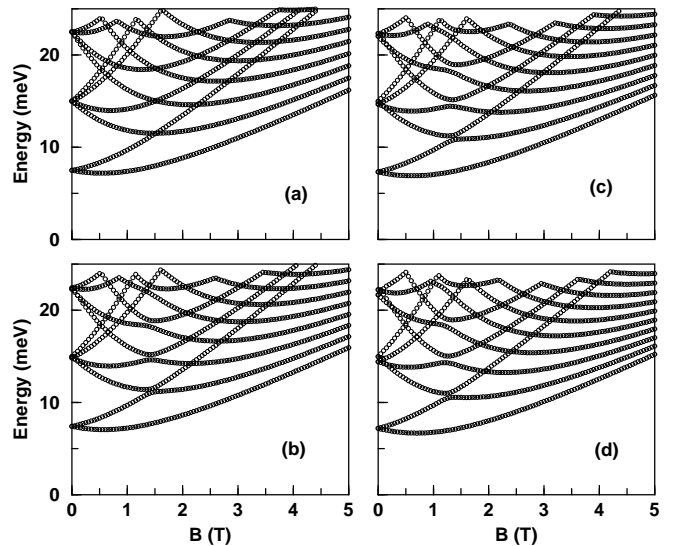


FIG. 2: Some of the low-lying energy states for non-interacting electrons confined in a InSb quantum dot for various values the SO coupling strength (in meV.nm), $\alpha = 0$ [a], $\alpha = 20$ [b], $\alpha = 30$ [c], and $\alpha = 40$ [d].

rule now applies to the total angular momentum J as well. Therefore, transitions from other states that are not allowed without the SO coupling, are now allowed.

B. Fock-Darwin spectra

In our numerical investigations, we choose InAs, InSb and GaAs quantum dots with parameters, $m^*/m_0 = 0.042$, $\epsilon = 14.6$, $g = -14$, $m^*/m_0 = 0.014$, $\epsilon = 17.88$, $g = -40$, and $m^*/m_0 = 0.063$, $\epsilon = 12.9$, $g = -0.44$, respectively. While the InAs quantum structures have been the system of choice for investigation of spin-related phenomena [34], InSb quantum dots are interesting for their very high g values and a relatively large α (~ 14 meV nm) [42]. For the GaAs quantum dots, the observed value of α is ~ 6 meV.nm [28]. In all these systems we consider the confinement potential strength to be $\hbar\omega_0 = 7.5$ meV. Some of the low-lying states of the Fock-Darwin spectra of the InAs, InSb and GaAs QDs are shown in Figs. 1 – 3 respectively and the corresponding optical absorption spectra in these systems are presented in Figs. 4 – 6.

As compared to the Fock-Darwin spectra of quantum dots without the SO coupling (shown in panels Figs. 1 – 3 [a]) the most outstanding features in the energy spectra of quantum dots with SO coupling are the *lifting of degeneracy* at zero magnetic field, the rearrangement of some of the levels at small fields and level repulsions at higher magnetic fields. To get some insight into the mechanism causing this kind of behavior, let us have a closer look, as an example, at the energy levels involved in the lowest absorption lines of the InAs dot [curves labelled “0” – “3” in Fig. 1 (a)].

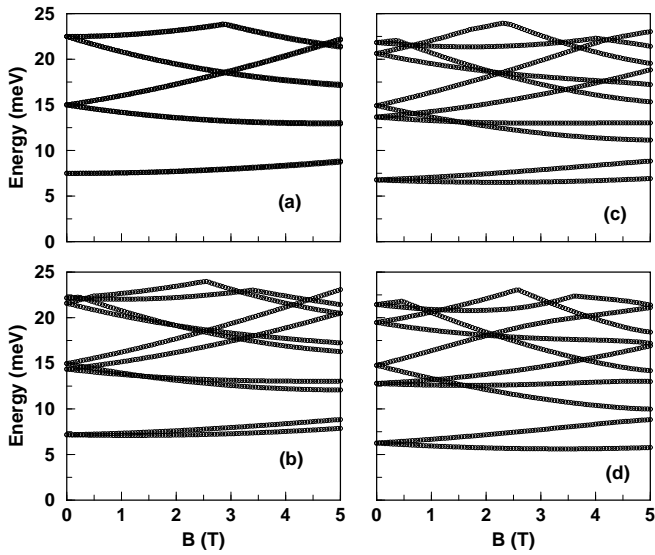


FIG. 3: Some of the low-lying energy states for non-interacting electrons confined in a GaAs quantum dot for various values the SO coupling strength (in meV.nm), $\alpha = 0$ [a], $\alpha = 20$ [b], $\alpha = 30$ [c], and $\alpha = 40$ [d].

	$g < 0$	$g > 0$
0	$\begin{pmatrix} \blacksquare e^{i0} \\ 0e^{i\theta} \end{pmatrix}$	$\begin{pmatrix} 0e^{-i\theta} \\ \blacksquare e^{i0} \end{pmatrix}$
1	$\begin{pmatrix} 0e^{-i\theta} \\ \blacksquare e^{i0} \end{pmatrix}$	$\begin{pmatrix} \blacksquare e^{i0} \\ 0e^{i\theta} \end{pmatrix}$
2	$\begin{pmatrix} \blacksquare e^{-i\theta} \\ 0e^{i0} \end{pmatrix}$	$\begin{pmatrix} 0e^{-2i\theta} \\ \blacksquare e^{-i\theta} \end{pmatrix}$
3	$\begin{pmatrix} \blacksquare e^{i\theta} \\ 0e^{2i\theta} \end{pmatrix}$	$\begin{pmatrix} 0e^{i0} \\ \blacksquare e^{i\theta} \end{pmatrix}$

TABLE I: Schematic spinors corresponding to four Fock-Darwin levels, marked 0 – 3 in Fig. 1 (a) of an InAs dot without SO coupling. The black rectangles stand for non-zero radial wave functions.

In the absence of the SO coupling energies of these levels are given by the formula (15). The corresponding spinors (schematic) are depicted in Table I, where the numbers in the first column refer to the labels in Fig. 1 (a). The spinors for electrons with negative and positive Lande' g -factors are shown in the middle and third columns respectively. In actual physical systems, conventionally only the spinors with $g < 0$ are of any interest.

The spinor states of electrons on lines 0 and 1 of Fig. 1 (a) differ only by the orientation of the spin: on line 0 the spin is parallel to the magnetic field ($\parallel \hat{z}$) while on line 1 the spin is antiparallel to the field. Thus the energy difference between these states is the Zeeman splitting. The total single-particle angular momenta (12) are cor-

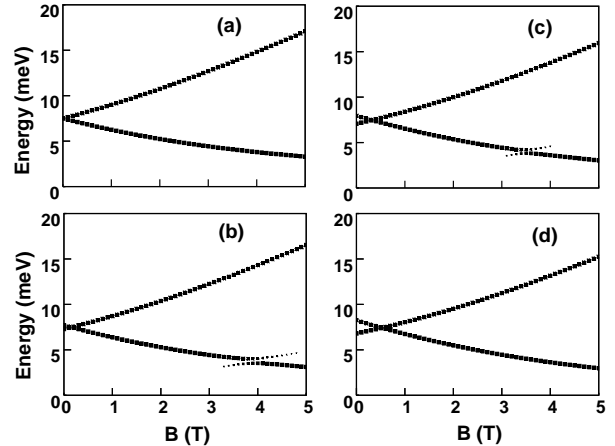


FIG. 4: Optical absorption spectra for non-interacting electrons confined in a InAs quantum dot for various values the SO coupling strength (in meV.nm), $\alpha = 0$ [a], $\alpha = 20$ [b], $\alpha = 30$ [c], and $\alpha = 40$ [d].

respondingly $j = \pm \frac{1}{2}$. Since under the SO coupling j is a good quantum number these two states will never mix even when the SO coupling is on. When the coupling strength α increases, the higher lying states with $j = \frac{1}{2}$ couple to the state 0 as well as states with $j = -\frac{1}{2}$ couple with the state 1. In Fig. 1 this shows up as an increasing splitting of the lines 0 and 1 when going through the panels from [a] to [d]. It should be noted, however, that the mixing has very minor effect on the ground state since the other states with $j = \frac{1}{2}$ are energetically very far from that.

Turning now our attention to electrons on lines 1 and 2 we see from the Table I (column $g < 0$) that their spinor states both have the same angular momentum $j = \ell + \frac{1}{2} = -\frac{1}{2}$. Consequently the SO interaction can mix these states. The mixing is particularly pronounced when the states are nearly degenerate, i.e. in the vicinity of the crossing point of lines 1 and 2. At moderate coupling strengths this mixing leads to level repulsions as shown in panels [b] and [c]. When the coupling is very strong, energetically higher states with $j = -\frac{1}{2}$ also become important in the mixing, leading to the imperceptibility of the level repulsion in panel [d].

We also mentioned lifting of degeneracies and rearrangements of energy levels as features of the SO coupling under small magnetic fields. Since we are interested in the absorption the most important states for us are the ones which can be reached from the ground state ($j = \frac{1}{2}$) respecting the dipole transition selection rule $\Delta j = \pm 1$. These are the lowest states with $j = -\frac{1}{2}$ and $j = \frac{3}{2}$ corresponding to the lines 2 and 3 in Fig. 1 (a) and to the spinors 2 and 3 (with $g < 0$) in Table I, respectively, for vanishing SO coupling. Since as the SO interaction is stronger the larger is the (angular) momentum of the electron, the spinor 3 possessing maximum orbital

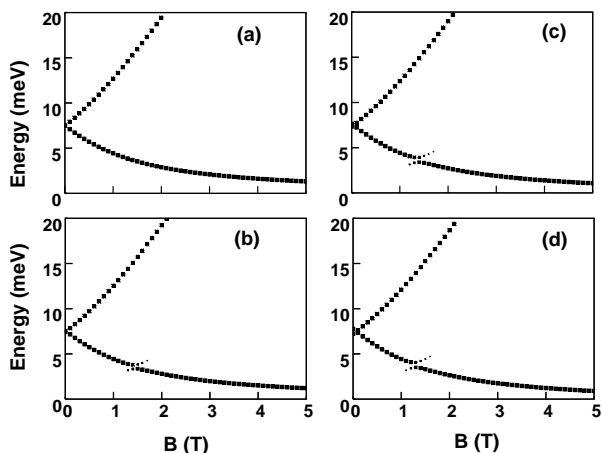


FIG. 5: Optical absorption spectra for non-interacting electrons confined in a InSb quantum dot for various values the SO coupling strength (in meV.nm), $\alpha = 0$ [a], $\alpha = 20$ [b], $\alpha = 30$ [c], and $\alpha = 40$ [d].

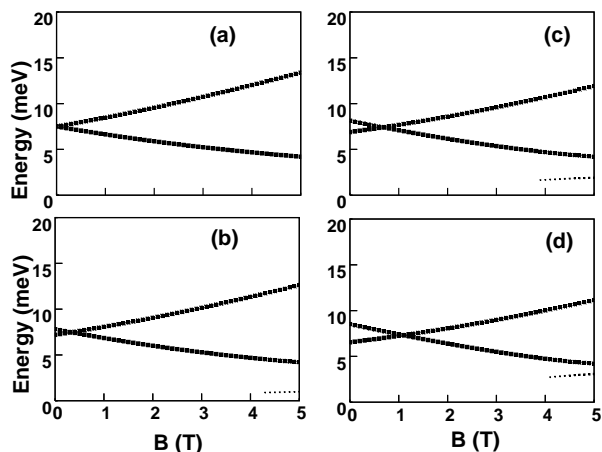


FIG. 6: Optical absorption spectra for non-interacting electrons confined in a GaAs quantum dot for various values the SO coupling strength (in meV.nm), $\alpha = 0$ [a], $\alpha = 20$ [b], $\alpha = 30$ [c], and $\alpha = 40$ [d].

angular momentum 2 is affected more than the spinor 2. Hence, although the energies of both spinors are decreased by the SO coupling the effect on the spinor 3 is larger.

Keeping the above discussions in mind it is now easy to interpret the features introduced by the SO coupling into the absorption spectra [Figs. (4 – 6)]. Firstly, although the lower absorption branch consists mainly of transitions from the state 0 to the state 2 it shows an anticrossing at moderate coupling strengths. This is a direct consequence of the mixing of the spinor states 1 and 2 which results in two spinors, both with nonzero upper component. Thus we can see transitions from the ground state 0 to both of these. Furthermore, as men-

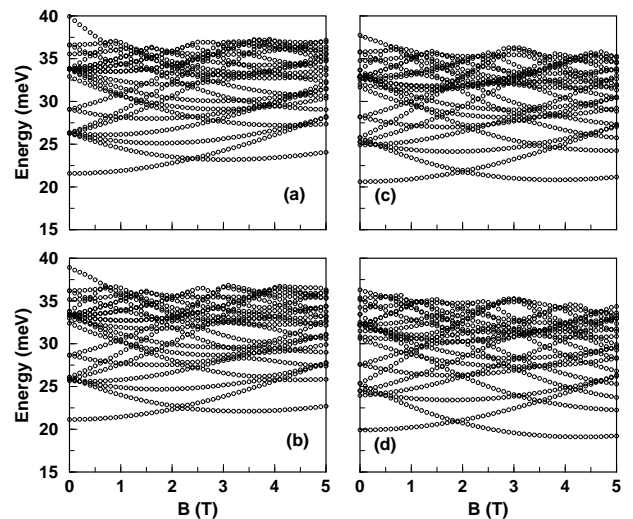


FIG. 7: Some of the low-lying energy states for two interacting electrons confined in a InAs quantum dot and for various values of the SO coupling strength (in meV.nm), α [meV nm]: (a) $\alpha = 0$, (b) $\alpha = 20$, (c) $\alpha = 30$, and $\alpha = 40$.

tioned earlier the level repulsion between states 1 and 2 resumes the form of level crossing when the SO interaction becomes very strong. This causes the anticrossing in the absorption spectra to disappear. In the InSb dot this happens already at $\alpha = 40$ while in the InAs dot the anticrossing still persists. Since the Lande' g -factor of GaAs is very small the Zeeman split state 1 does not meet the state 2 within the range of the magnetic field under consideration. Consequently we see at the lower right corners of Fig. 6 (b) – (d) only the beginnings of the lower branches of these anticrossings.

Secondly, the upper absorption branch corresponds mainly to transitions from the state 0 to the state 3 modified by the SO coupling. The small magnetic field however makes an exception. As we discussed above, at small fields the state 3 is energetically lower than the state 2 due to the SO interaction. Thus we get a crossing of spectra at small fields.

From Eq. (15), the separation between the states 2 and 3, and hence also the gap between the absorption line branches is roughly proportional to the cyclotron frequency ω_c which in turn is linearly proportional to the magnetic field and inversely proportional to the effective mass of the electron. Thus, due to the very small effective mass of the electron in an InSb dot the energy of the spinor 3 exceeds the energy of the spinor 2 already at very small magnetic fields. Consequently also the crossing of absorption lines of an InSb dot occurs at very small magnetic fields as can be seen in Figs. 5 (b)-(d).

At this point it may be worth mentioning that the energetics of the single-electron quantum dot under the influence of the SO coupling and subjected to an external magnetic field depends strongly on the sign of the Lande' g -factor. This is contrary to the case without SO

coupling where the energy spectrum is independent on the sign of g although, of course, the orientation of spin is determined by it. Let us consider, for example, the lowest absorption branch in the case $g > 0$. From Table I we can deduce that also in this case the transitions mainly take the spinor 0 to the spinor 2. Now, however, there is no spinor level which would cross or even come close to the energy of the state 2 and mix with it. Consequently the anticrossing described above would not be observable in this case.

This concludes our discussion of the energy levels and optical absorption spectra in a non-interacting QD in a magnetic field and in the presence of SO interaction. In what follows, we describe the theory for a interacting few-electron parabolic quantum dot.

III. MANY-ELECTRON SYSTEMS

The basis \mathcal{B}_N for N interacting electrons in a QD is constructed as a direct antisymmetrized product of single-particle basis \mathcal{B}_S (27) of the form

$$\begin{aligned} \mathcal{B}_N &= \mathcal{A} \bigotimes_{j=1}^N \mathcal{B}_S = \{ |\Lambda_i\rangle | i = 1, 2, \dots \} \\ &= \{ |\lambda_{i_1}; \lambda_{i_2}; \dots; \lambda_{i_N}\rangle | i_j = 0, 1, 2, \dots \} \\ &= \{ |k_1, \ell_1; \dots; k_N, \ell_N\rangle | k_j = 0, 1, \dots; \\ &\quad \ell_j = 0, \pm 1, \dots \}, \end{aligned} \quad (32)$$

where \mathcal{A} stands for the antisymmetrization operator. It is also understood that the notations such as $|\lambda_{i_1}; \lambda_{i_2}; \dots; \lambda_{i_N}\rangle$ represent the antisymmetrized direct

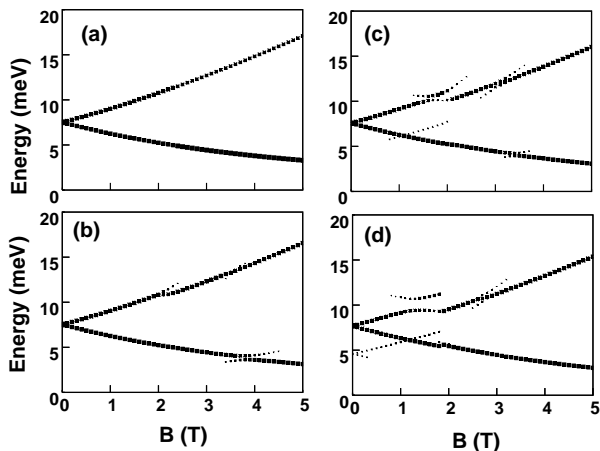


FIG. 8: Dipole-allowed transition energies for two interacting electrons confined in a InAs quantum dot and for various values of the SO coupling strength (in meV.nm), α [meV nm]: (a) $\alpha = 0$, (b) $\alpha = 20$, (c) $\alpha = 30$, and (d) $\alpha = 40$. The size of the points in the figures is proportional to the calculated intensity.

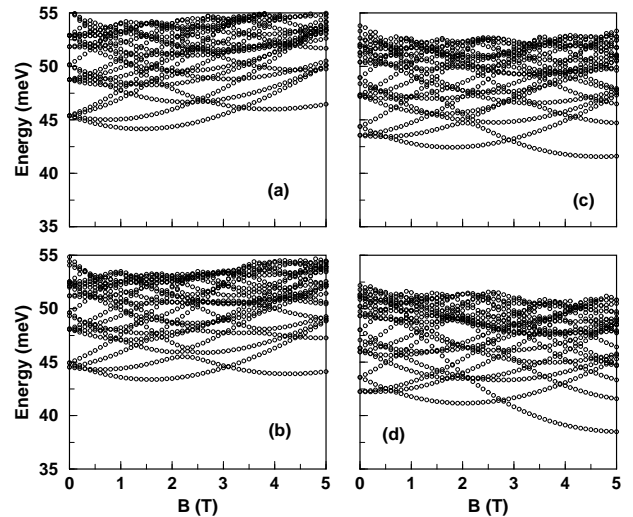


FIG. 9: Same as in 7 but for a three-electron InAs quantum dot.

products, i.e.,

$$|\Lambda_q\rangle = |\lambda_{i_1}; \lambda_{i_2}; \dots; \lambda_{i_N}\rangle = \mathcal{A} [|\lambda_{i_1}\rangle \otimes |\lambda_{i_2}\rangle \otimes \dots \otimes |\lambda_{i_N}\rangle]. \quad (33)$$

Usually it is possible to restrict the size of \mathcal{B}_N using the conservation laws. For example, in a rotationally invariant system the total angular momentum is a good quantum number. Therefore, for example, we fix it to J , and accept into the basis only those states that satisfy

$$\sum_{i=1}^N j_i = J.$$

The states of the interacting system are expressed as superposition of the non-interacting states taken from the basis set (32)

$$|\Psi\rangle = \sum_{i=1} c_i |\Lambda_i\rangle. \quad (34)$$

To extract the coefficients c_i , we again resort to the minimization, i.e. we minimize the Rayleigh quotient

$$\rho = \frac{\langle \Psi | \mathcal{H} | \Psi \rangle}{\langle \Psi | \Psi \rangle},$$

where \mathcal{H} is the total many-body Hamiltonian. Again this leads to the diagonalization of the Hamiltonian matrix with elements $\langle \Lambda_i | \mathcal{H} | \Lambda_j \rangle$. The eigenvectors are the desired expansion coefficients and the eigenvalues the corresponding energies of the interacting system. It will be clear from the Appendix that both these tasks, construction of the Hamiltonian matrix and its diagonalization are numerically quite challenging.

A. Coulomb matrix elements

We write the total Hamiltonian \mathcal{H} as a sum of the single-particle operators (4) and two-body operators $V(\vec{r}, \vec{r}')$ as

$$\mathcal{H} = \sum_{i=1}^N \mathcal{H}_0(\vec{r}_i) + \frac{1}{2} \sum_{i \neq j}^N V(\vec{r}_i, \vec{r}_j). \quad (35)$$

Since our basis states $|\Lambda_i\rangle$ are diagonal by construction in \mathcal{H}_0 we only need to evaluate the matrix elements of the latter sum in (35). Our many-body states $|\Lambda_i\rangle$ are expressed in occupation representation language (33), and therefore it is natural to proceed in the occupation number space. This means that for the interaction part we have to evaluate the two-body terms

$$V_{\lambda_1 \lambda_2 \lambda_3 \lambda_4} = \langle \lambda_1 \lambda_2 | V | \lambda_3 \lambda_4 \rangle. \quad (36)$$

In our system the mutual interaction between the electrons is taken to be purely Coulombic, i.e.

$$V(\vec{r}, \vec{r}') = \frac{e^2}{\epsilon |\vec{r} - \vec{r}'|} \quad (37)$$

where ϵ is the effective dielectric constant of the material. The interaction operator is thus diagonal in spin. Recalling that our single-particle states $|\lambda\rangle$ were two-component spinors (8), the two-body term (36) consists of sum of four terms and is of the form

$$V_{\lambda_1 \lambda_2 \lambda_3 \lambda_4} = \sum_{\sigma, \sigma'} \int d\vec{r} d\vec{r}' \phi_1^{\sigma*}(\vec{r}) \phi_2^{\sigma'*}(\vec{r}') V(\vec{r}, \vec{r}') \phi_3^{\sigma'}(\vec{r}') \phi_4^{\sigma}(\vec{r}) \quad (38)$$

where the summation indices take values \uparrow and \downarrow . Furthermore, since we expressed the spatial components ϕ^σ as superpositions of functions $g_{n\ell} e^{i\ell\theta}$ [Eq. (17)],

$$g^{\uparrow, \downarrow} = \sum_{n=0} c_{n, \ell}^{\uparrow, \downarrow} g_{n, \ell},$$

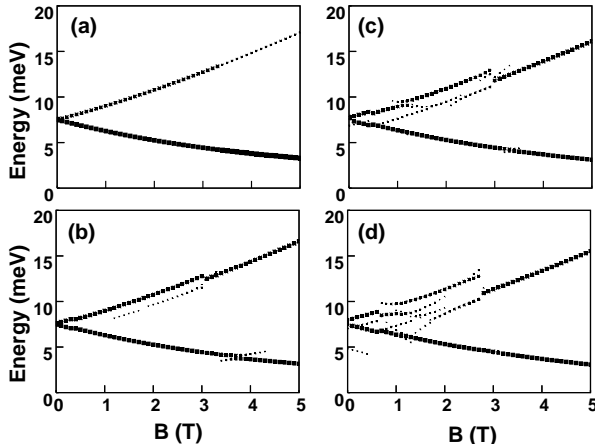


FIG. 10: Same as in Fig. 8, but for a three-electron InAs quantum dot.

we are ultimately led to evaluate the Coulomb matrix elements in the oscillator wavefunction

$$w_{n\ell}(\vec{r}) = g_{n\ell} e^{i\ell\theta} = \sqrt{\frac{n!}{(n+|\ell|)!}} e^{-x/2} x^{|\ell|/2} L_n^{|\ell|}(x) e^{i\ell\theta}$$

basis. These matrix elements can be expressed in terms of finite sums as [4]

$$\begin{aligned} \mathcal{A}_{n_1 n_2 n_3 n_4} &= \langle w_{n_1 \ell_1} w_{n_2 \ell_2} | \frac{e^2}{\epsilon |\vec{r} - \vec{r}'|} | w_{n_3 \ell_3} w_{n_4 \ell_4} \rangle \\ &= \delta_{\ell_1 + \ell_2, \ell_3 + \ell_4} \frac{\sqrt{2} e^2}{\epsilon a} \left[\frac{n_1!}{(n_1 + |\ell_1|)!} \right]^{\frac{1}{2}} \\ &\quad \times \left[\frac{n_2!}{(n_2 + |\ell_2|)!} \right]^{\frac{1}{2}} \left[\frac{n_3!}{(n_3 + |\ell_3|)!} \right]^{\frac{1}{2}} \left[\frac{n_4!}{(n_4 + |\ell_4|)!} \right]^{\frac{1}{2}} \\ &\quad \times \sum_{\kappa_1=0}^{n_1} \sum_{\kappa_2=0}^{n_2} \sum_{\kappa_3=0}^{n_3} \sum_{\kappa_4=0}^{n_4} [\kappa_1 + \kappa_4 + \frac{1}{2}(|\ell_1| + |\ell_4| - k)]! \\ &\quad \times [\kappa_2 + \kappa_3 + \frac{1}{2}(|\ell_2| + |\ell_3| - k)]! \\ &\quad \times \frac{(-1)^{\kappa_1 + \kappa_4}}{\kappa_1! \kappa_4!} \frac{(n_1 + |\ell_1|)! (n_4 + |\ell_4|)!}{(n_1 - \kappa_1)! (|\ell_1| + \kappa_1)! (n_4 - \kappa_4)! (|\ell_4| + \kappa_4)!} \\ &\quad \times \frac{(-1)^{\kappa_2 + \kappa_3}}{\kappa_2! \kappa_3!} \frac{(n_2 + |\ell_2|)! (n_3 + |\ell_3|)!}{(n_2 - \kappa_2)! (|\ell_2| + \kappa_2)! (n_3 - \kappa_3)! (|\ell_3| + \kappa_3)!} \\ &\quad \times \sum_{s=0}^{\kappa_{14}} \frac{[\kappa_1 + \kappa_4 + \frac{1}{2}(|\ell_1| + |\ell_4| + k)]!}{[\kappa_1 + \kappa_4 + \frac{1}{2}(|\ell_1| + |\ell_4| - k) - s]! (k + s)!} \\ &\quad \times \sum_{t=0}^{\kappa_{23}} \frac{[\kappa_2 + \kappa_3 + \frac{1}{2}(|\ell_2| + |\ell_3| + k)]!}{[\kappa_2 + \kappa_3 + \frac{1}{2}(|\ell_2| + |\ell_3| - k) - t]! (k + t)!} \\ &\quad \times \frac{(-1)^{s+t}}{s! t!} \cdot \frac{\Gamma(k + s + t + \frac{1}{2})}{2^{k+s+t+1}}, \end{aligned} \quad (39)$$

where $\kappa_{14} = \kappa_1 + \kappa_4 + \frac{1}{2}(|\ell_1| + |\ell_4| - k)$, $\kappa_{23} = \kappa_2 + \kappa_3 + \frac{1}{2}(|\ell_2| + |\ell_3| - k)$ and $k = |\ell_1 - \ell_4| = |\ell_2 - \ell_3|$. Numerical techniques to evaluate these two-body terms and to diagonalize the resulting Hamiltonian matrix is described in the Appendix.

IV. RESULTS AND DISCUSSIONS

For numerical evaluation of the energy spectra and the optical absorption spectrum for QDs with a few interacting electrons, we have considered the InAs, InSb and GaAs quantum dots. Parameters of these systems are already given in Sect. II. The energy spectra and the optical absorption spectra for these systems are described in the subsections below.

A. InAs quantum dots

Our numerical results for energy spectra and absorption spectra (dipole-allowed) for 2 – 4 electrons are presented in Figs. 7-12, and for various values of the SO

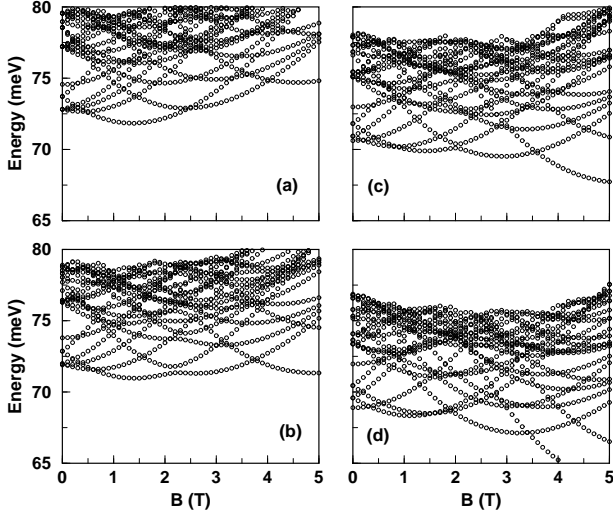


FIG. 11: Same as in 7 but for a four-electron InAs quantum dot.

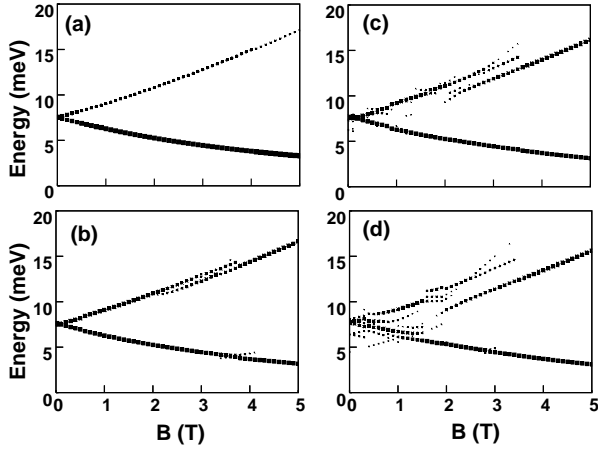


FIG. 12: Same as in Fig. 8, but for a four-electron InAs quantum dot.

coupling strength (in meV.nm), α . As in the case of the non-interacting electron system, we have considered the following parameters for the InAs quantum dot: $m^*/m_0 = 0.042$, $\epsilon = 14.6$, $g = -14$ and $\hbar\omega_0 = 7.5$ meV.

A striking feature visible in the absorption spectra (Figs. 8, 10, and 12) is the appearance of discontinuities, anticrossings and new modes in addition to the two main ($\alpha = 0$) absorption lines. These optical signatures of the SO interaction are consequences of the multitude of level crossings and level repulsions that occur in the energy spectra (Figs. 7, 9, and 11). The latter ones can be attributed to an interplay between the SO and Zeeman couplings. In order to understand their origin, let us first examine the case of the two-electron system (Figs. 7,8). In our spinor notation the main contribution to the ground state at zero magnetic field comes from the

two-electron state $|\lambda_{\ell_1}, \lambda_{\ell_2}\rangle = |\lambda_0, \lambda_{-1}\rangle$, where $|\lambda_{\ell_1}\rangle$ is a spinor with $j_1 = \ell_1 + 1/2 = 1/2$, $d_n^{\lambda_1} = 0$, and $|\lambda_{\ell_2}\rangle$ a spinor with $j_2 = -1/2$ and $u_n^{\lambda_2} = 0$, i.e., both electrons have zero orbital angular momenta with opposite spins (corresponding to the spinors 0 and 1 in Table I with $J = j_1 + j_2 = 0$). When we increase the magnetic field the spin triplet configuration will become, due to the interaction, energetically more favorable. If the Lande' g -factor is negative then the electrons would like to occupy states with orbital angular momenta 0 and -1 with both spins up (i.e., states 0 and 2 of Table I). In the spinor picture this means that $|\lambda_{\ell_2}\rangle$ still has $\ell_2 = -1$ ($J = 0$) but now $u_n^{\lambda_2} \neq 0$ and $d_n^{\lambda_2} = 0$. The SO interaction mixes these two configurations which results in a level repulsion. On the other hand, when the strength of the SO coupling is further increased, the relative significance of the Zeeman contribution to \mathcal{H}_0 decreases. The energy shifts to states with $J \neq 0$ will then become energetically feasible and we again have crossings of levels. For increasing number of electrons in the dot, the energy spectra is more dense and exhibit additional level crossings (Figs. 9 – 12). As a consequence, the ground state angular momentum also changes more frequently as compared to that of the two-electron case. It should be pointed out that in many-electron dots these level crossings and repulsion are to be attributed, at least partly to the mutual Coulomb interactions. The level crossings/repulsions we saw earlier [e.g. levels 1 and 2 in Fig. 1 (a)] in the single-particle picture are due to the Zeeman splitting whereas in interacting systems crossings occur even in the limit of vanishing Zeeman coupling. In the present InAs dot the Coulomb interaction brings, for example the singlet-triplet transition to much lower magnetic field ($B \approx 2$ T) as compared to the field required in a noninteracting system ($B \approx 4$ T).

At moderate SO coupling strengths the absorption

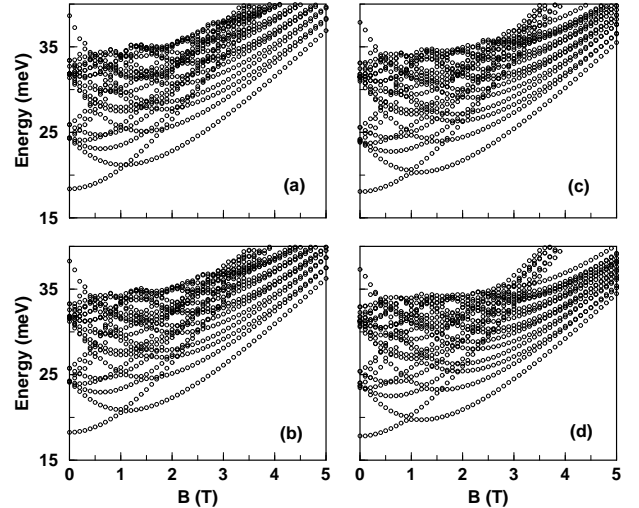


FIG. 13: Same as in 7 but for a two-electron InSb quantum dot.

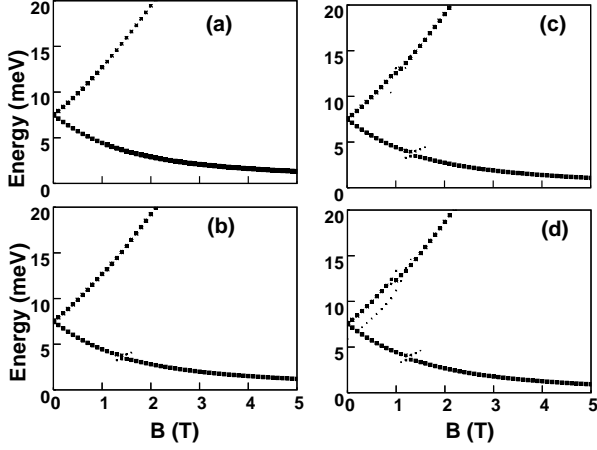


FIG. 14: Same as in Fig. 8, but for a two-electron InSb quantum dot.

spectra do not essentially differ from the single-particle spectrum. But when the coupling strength increases the deviation from the pure parabolic confinement also increases which in turn implies that the lowest final states of dipole allowed transitions are not any more achievable by adding $\hbar\Omega \pm \frac{1}{2}\hbar\omega_c$ to the initial state energies. In particular, this results in discontinuities and anticrossing behaviors as well as appearance of new modes. As an illustration, let us consider the absorptions that at a magnetic field of $B = 1$ T take the two-electron system from the ground state to excited states. In the absence of the SO coupling the ground state is a spin-singlet state $S = 0$ with total angular momentum $J = 0$. According to the dipole selection rules absorptions cause transitions to states $J = \pm 1$ and $S = 0$ with energies ΔE_{\pm} above the ground state. In Fig. 8 (d), we note that in addition

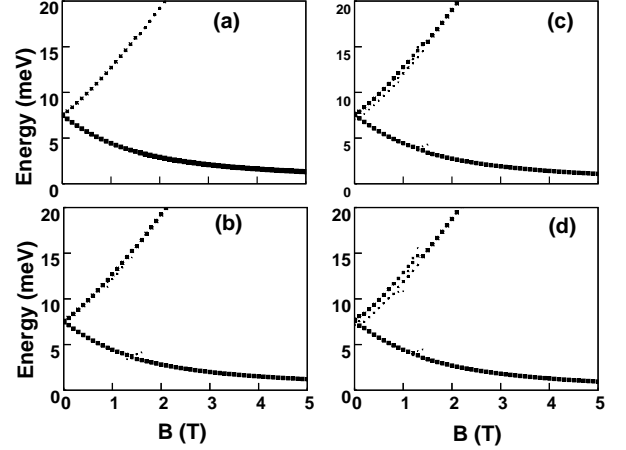


FIG. 16: Same as in Fig. 8, but for a three-electron InSb quantum dot.

to the two main lines there are now two additional lines (at around $B = 1$ T) of appreciable intensity at the SO coupling strength $\alpha = 40$ (meV.nm). Further analysis reveals that the ground states still have $J = 0$ and that the expectation value of the spin z -component is $\langle\sigma_z\rangle = 0$. The excited states also have $J = \pm 1$, as before. However, the final spin states can no longer be classified as singlets: the expectation values $\langle\sigma_z\rangle$ vary between -0.03 and 0.39 . When the number of electrons increases the number of these additional modes also increases but at the same time the relative intensities decrease (at each B we have normalized the total intensity to unity). On the other hand, the discontinuities as consequences of deviations from a parabolic confinement become more pronounced (Figs. 9 – 12). This is because there are higher angular

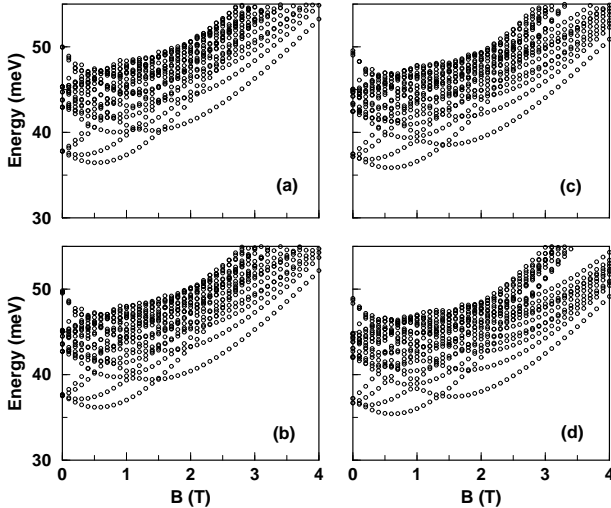


FIG. 15: Same as in 7 but for a three-electron InSb quantum dot.

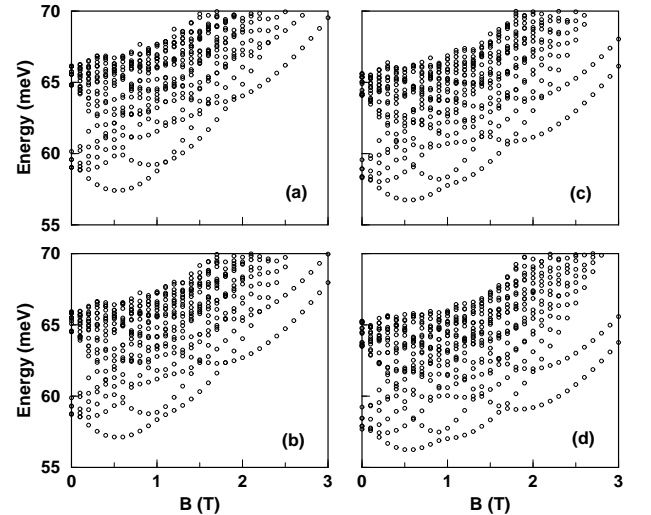


FIG. 17: Same as in 7 but for a four-electron InSb quantum dot.

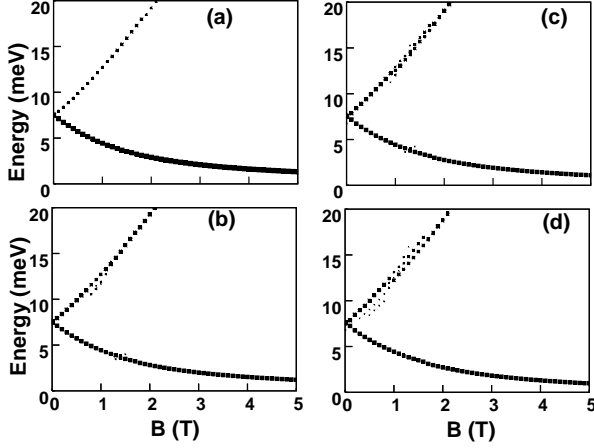


FIG. 18: Same as in Fig. 8, but for a four-electron InSb quantum dot.

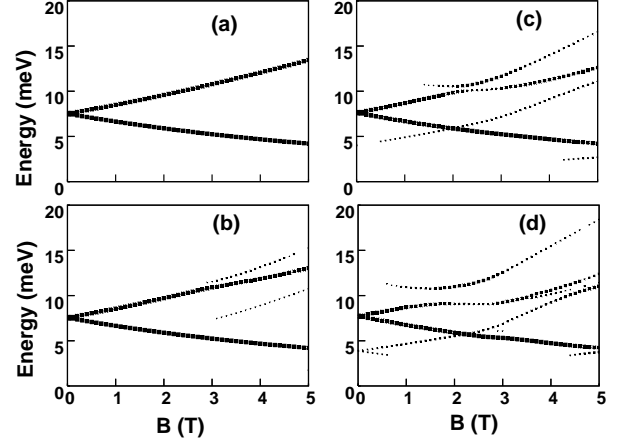


FIG. 20: Same as in Fig. 8, but for a two-electron GaAs quantum dot.

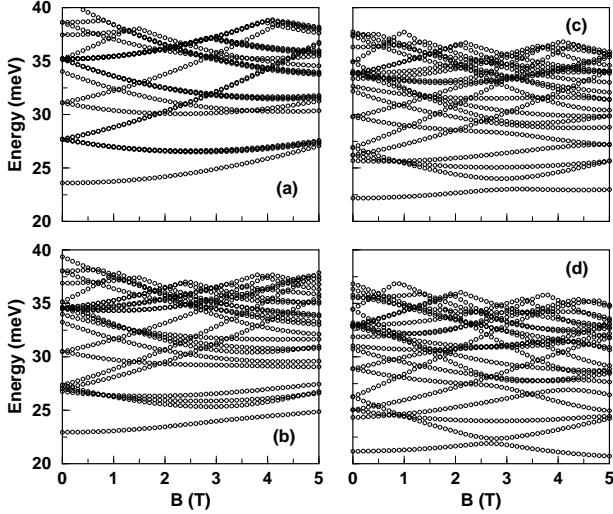


FIG. 19: Same as in 7 but for a two-electron GaAs quantum dot.

momenta involved in the dipole transitions. As a consequence of this the upper absorption branch now exhibits a rich structure while in the single-particle picture it is practically featureless.

B. InSb quantum dots

As mentioned above, in addition to the InAs quantum dots, investigation of InSb quantum dots are also thought to be interesting, particularly in the context of SO coupling effects due to the large values of $|g|$ and α [42]. We have considered the following parameters for the InSb quantum dot: $m^*/m_0 = 0.014$, $\epsilon = 17.88$, $g = -40$ and $\hbar\omega_0 = 7.5$ meV. The energy levels for InSb quantum dots containing 2 – 4 interacting electrons are plotted in

Figs. 13, 15, 17 and for various values of the SO coupling strength α . The corresponding optical absorption spectra are presented in Figs. 14, 16, and 18. As compared to the spectra of InAs dots a clear difference is the almost total absence of anticrossings and discontinuities. This is partly due to the very large Zeeman coupling which practically nullifies the SO interaction at the coupling strengths α we are concerned with. Another reason is the large kinetic energies due to the very small electron effective mass. Because the strength of the Coulomb interaction is somewhat smaller than in InAs ($\epsilon_{\text{InSb}} > \epsilon_{\text{InAs}}$) correlations caused by the mutual electronic interactions are effectively much smaller in InSb than in InAs. For the exploration of the SO coupling via absorption spectroscopy, InSb quantum dots do not seem to be a very promising system.

C. GaAs quantum dots

The results for GaAs quantum dots, ones that are most intensely explored in the absence of SO coupling, are presented here primarily as an academic interest. The parameters that we have used here are: $m^*/m_0 = 0.063$, $\epsilon = 12.9$, $g = -0.44$ and $\hbar\omega_0 = 7.5$ meV. Clearly, the very low value of the $|g|$ -factor perhaps makes the GaAs QDs unsuitable for any observable effect due to the SO coupling. Interestingly, however, among all the three types of QDs studied here for optical absorptions, GaAs QDs show the most spectacular effects for large values of α . The energy levels for GaAs quantum dots containing 2 – 4 interacting electrons are plotted in Figs. 19, 21, and 23 for various values of the SO coupling strength α . The corresponding optical absorption spectra are presented in Figs. 20, 22, and 24 respectively. As mentioned above, the only observed value of α for GaAs QD reported as yet is $\alpha \sim 6$ meV.nm [28]. Reversing the arguments presented in the previous subsection, i.e. in GaAs a very small Zeeman

coupling and a rather large effective electron mass but practically equal strength of Coulomb interaction help us understand why the absorption spectra of our GaAs dots exhibit a remarkably rich structure as opposed to those of the InSb and InAs dots. Finding an appropriate set up to generate a large α for GaAs quantum dot would be a major (but worthwhile) experimental endeavor.

V. A BRIEF REVIEW OF EARLIER THEORETICAL WORKS

In this section, we present a critical review of earlier theoretical reports on how the Bychkov-Rashba spin-orbit coupling in parabolic quantum dots were treated [14, 15, 16, 17, 18, 19, 20, 21, 22, 23, 24, 25, 26, 27, 28, 29, 30]. There are quasi-exact solutions available for electrons confined in a parabolic quantum dot in the presence of the SO interaction, but without the inter-electron interaction [19], and exact analytical results are also reported in the case of a circular quantum dot with hard walls [20], again for a non-interacting system, but with the Bychkov-Rashba spin-orbit interaction included. However, for the realistic systems of parabolic quantum dots with interacting electrons these methods are prohibitively complicated and evaluation of the energy spectrum can only be done numerically. Among the theoretical papers dealing with the SO interaction in quantum dots discussed below, Kuan et al. [14] presented the best treatment of the single-electron states. They looked at the energy levels of parabolically confined quantum dots with Bychkov-Rashba SO coupling and in the presence of zero and nonzero magnetic fields. They solved the single-particle equation correctly by expanding the solution spinors in terms of the eigenfunctions of QDs without the SO interaction, i.e. the Laguerre functions. We have used a similar approach to construct the basis states for our multi-electron QDs [Sects. II, III].

Voskoboynikov et al. [15] studied the effect of SO interaction on the energy spectrum of cylindrical semiconductor QDs in an externally applied magnetic field. They considered the Bychkov-Rashba SO coupling due to the parabolic confinement, i.e. an in-plane field conserving orbital and spin angular momenta. As a consequence, the SO coupling has no qualitative effects on, for example, the absorption spectra. The electron-electron interaction was not included in this scheme. In Ref. [16], they studied the magnetization and magnetic susceptibility in few-electron parabolic QDs with SO coupling. As in their earlier paper, they handled the SO term only due to the parabolic confinement and therefore the single-particle Hamiltonian is diagonal in spin space. They neglected the mutual electronic Coulomb interaction.

Governale [17] investigated the effects of SO coupling on the addition energy and on the spin properties of few-electron QDs in the absence of the external magnetic field. He introduced the SO coupling into single-particle states perturbatively but also compared the resulting en-

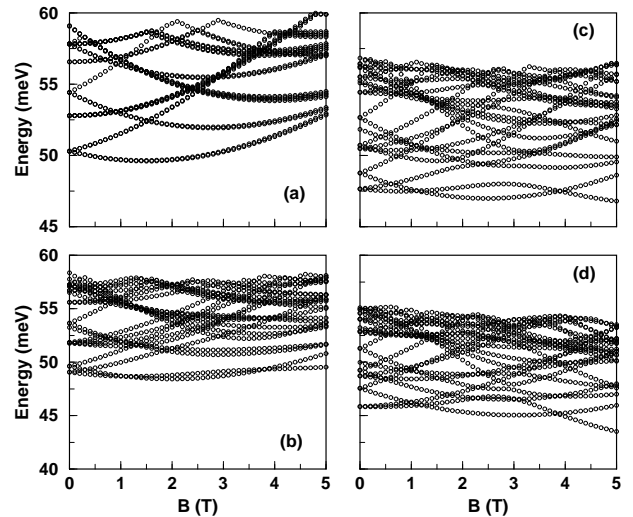


FIG. 21: Same as in 7 but for a three-electron GaAs quantum dot.

ergies to the ones obtained by numerical diagonalization technique. At the small SO coupling strength that he considered, the perturbation approach seems to be valid. Electron correlations were handled by using the spin-density functional approach. Cremers et al. [18] studied conductance and its fluctuations in the presence of SO interaction, Zeeman coupling, externally applied magnetic field, in a (single-electron) QD. They solved the single-particle equation applying an approximate unitary transformation which in leading order takes the Hamiltonian to a diagonal form in spin space.

Valin-Rodriguez [21] considered a single electron in a parabolic QD with Bychkov-Rashba SO coupling. He performed a unitary transformation to transform the Hamiltonian in spin space to a diagonal form up to second

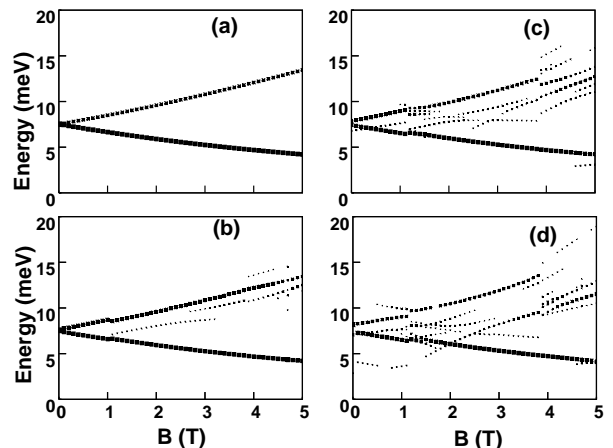


FIG. 22: Same as in Fig. 8, but for a three-electron GaAs quantum dot.

order in SO and Zeeman coupling parameters. He showed that the effective SO interaction is influenced by the interplay between Zeeman and SO couplings. In Ref. [22], Valin-Rodriguez et al. introduced a spatially modulated (in radial direction) Bychkov-Rashba coupling in single-electron (disk) QDs. They solved the two-component spinor equation and numerically evaluated the spin density. They concluded that it is possible to confine electrons spatially with appropriate structural modulation. These authors also investigated the SO couplings in deformed parabolic quantum dots [23]. They solved the single-particle equations using the approximate unitary transformations mentioned above. They were interested in the effects of spatial deformations to the spin splitting oscillations. They estimated the Coulomb interaction contribution using the time-dependent local-spin-density approximation [24].

Lucignano et al. [25] studied the few-electron QDs including the mutual electron-electron interaction and under the influence of an externally applied magnetic field. They applied an exact diagonalization method (but with a rather restricted basis: 28 single-particle states deducing from their earlier paper [43]). They particularly looked at the possibility to use the SO coupling to control the excitations under the magnetic fields which polarize the ground state, i.e., close to the final *single-triplet* transition. The SO coupling is included in the many-electron Hamiltonian, but not in the basis states. They evaluated the dipole matrix elements for absorption from the ground state to the lowest dipole-allowed excited state. They claimed that there is an increase in intensity close to the transition to the fully polarized ground state.

Destefani et al. [26] reported numerical results for energy levels and spin polarizations for one and two-electron parabolic QDs under a magnetic field and the SO coupling. For the two-electron system, Coulomb in-

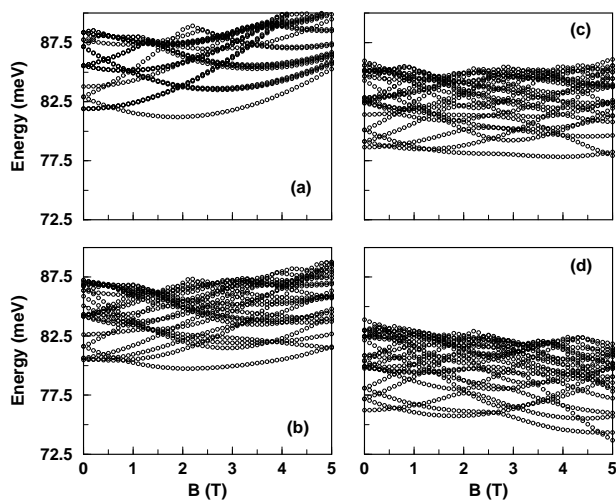


FIG. 23: Same as in 7 but for a four-electron GaAs quantum dot.

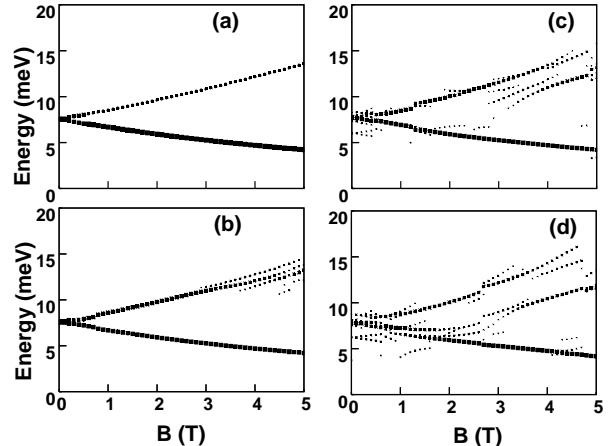


FIG. 24: Same as in Fig. 8, but for a four-electron GaAs quantum dot.

teraction is also included. They do not construct the correct single-electron states in the two-electron QD, the SO coupling is, in fact, taken into account only in the many-electron Hamiltonian. DeBald et al. [27] studied oscillations in few-electron parabolic QD in a magnetic field, between states where the degeneracy is lifted by the SO coupling, i.e. at the level repulsion points. The Coulomb interaction was taken into account only approximately, because the many-body effects were claimed to play only a minor role in the very small magnetic field considered in that work. Könemann et al. [28] considered the SO coupling in single electron QDs. They showed that there is an anisotropy between spin splittings due to magnetic fields parallel and perpendicular to the dot. The anisotropy was shown to be proportional to the strength of the SO coupling. Bellucci and Onorato [29] studied the influence of SO coupling on the charge and spin polarization in a vertical disk-shaped QD under a strong perpendicular magnetic field. They treated the SO coupling perturbatively (upto second order). They handled the Coulomb interaction within the Hartree-Fock approach. They studied the energy splittings due to the SO coupling. Finally, Fransson et al. [30] studied transport through QDs with spin dependent couplings to the contacts. They evaluated the QD energy levels using a (first principles) density functional theory. They calculated the transport properties of (a) non-interacting electrons taking into account the few levels closest to the Fermi level, and (b) interacting electrons using an approximate Hamiltonian with the levels closest to the Fermi level. We would like to note here that, in the light of all these theoretical approaches, our method of including the SO coupling for interacting electrons in a parabolic QD seems to be the most accurate one. Although, given the fact that our approach involves extensive numerical computations, some of the approaches discussed above, such as the one by Lucignano et al. [25], seem to be very promising.

VI. CONCLUSIONS

In conclusion, we have studied the energy levels and optical-absorption spectra for parabolic quantum dots containing upto four interacting electrons, in the presence of spin-orbit coupling and under the influence of an externally applied, perpendicular magnetic field. We have presented a very accurate numerical scheme to evaluate these quantities. We have presented results for the Fock-Darwin spectra in the presence of SO coupling for quantum dots made out of three different semiconductor systems, InAs, InSb, and GaAs. The effects of SO coupling on the single-electron spectra are primarily to lift the degeneracy at $B = 0$, rearrangement of some of the energy levels at small magnetic fields, and level repulsions at high fields. These are explained as due to mixing of different spinor states for increasing strength of SO coupling. As a consequence, the corresponding absorption spectra reveal anticrossing structures in the two main lines ($\alpha = 0$) of the spectra. For the interacting many-electron systems we observed the appearance of discontinuities, anticrossings, and new modes that appear in conjunction with the two main absorption lines. These additional features arise entirely due to the SO coupling and are a consequence of level crossings and level repulsions in the energy spectra. An intricate interplay between the SO coupling and the Zeeman energies are shown to be responsible for these new features seen in the energy spectra. Our accurate results for the low-lying energy levels for the SO coupled QDs can also be measured, in principle, by transport [38] or capacitance [39] spectroscopy, which have been successfully employed earlier to map out the energy spectra of parabolic quantum dots. Optical absorption spectra for all three types of quantum dots containing a few interacting electrons that are studied here show a common feature: new modes appear, mostly near the upper main branch of the spectra around 2 tesla that become stronger with increasing α . Among the three types of systems considered here, optical signatures of the SO interaction is found to be the strongest in the absorption spectra of a GaAs quantum dot, but only at very large values of the SO coupling strength, and appears to be the weakest for the InSb quantum dots. Experimental observation of these new optical modes that appear solely due to the presence of SO coupling would be very exciting because that would be a major step forward in our quest to manipulate the spin dynamics in nanostructured systems via the SO coupling.

Our future works along this line will be to explore coupled QDs, or QD molecules [44]. Our primary goal will be to generate accurate results for energy levels and optical absorption spectra for coupled (laterally [45] or vertically [46]) quantum dots with spin-orbit interaction. In addition to being important for fundamental studies, these results would be interesting from the point of view of quantum computations [47] as well. It is now well recognized that semiconductor quantum dots have the poten-

tial to become the building blocks for solid state quantum computation. Quantum states of single, double and even triple coupled [48] quantum dots have been explored for this purpose. In a quantum computer, information is stored in a two-level system. Hence a promising candidate system to realize the quantum bits, the fundamental unit of information in a quantum computer, is a quantum dot where the single-electron states can be used for that purpose. In a magnetic field, the Zeeman splitting of electron spin can provide a two-level system (for an odd number of electrons). Alternatively, the spatial wave function of a single-electron state in a double quantum dot (allowing for electron tunneling between the two dots) can also represent a two-level system. Spin-orbit coupling in the coupled quantum dot systems could perhaps be used to perform quantum computation (using the spin rotation, for example). Accurate results for the energy levels of the coupled-dot system might be beneficial in that direction of research. The effects of SO coupling on the energy levels and absorption spectra for a more complex system such as coupled QDs are, however, important and interesting in their own ways. These would be the subjects of our future publications.

VII. ACKNOWLEDGMENTS

The work of T.C. has been supported by the Canada Research Chair Program and the Canadian Foundation for Innovation (CFI) Grant. We wish to thank Dr. Alex Voskoboinikov for a critical reading of the manuscript.

APPENDIX: DIAGONALIZATION OF MONSTER MATRICES

We have mentioned in Sect. III about the challenging task of construction of the Hamiltonian matrix and its numerical diagonalization. Here we present a brief discussion about the numerical method that we believe the most accurate (and appropriate) for that task. While in principle, evaluation of Eq. (39) is straightforward it turns out to be numerically highly unstable, primarily due to the expansion (17) extending to Laguerre polynomials of large degree and large angular momenta which in turn, leads to large terms of alternating sign [49]. A remedy for this is to employ multiple precision arithmetics such as, for example implemented in the Gnu arbitrary precision GMP library. However, if we apply multiple precision arithmetic directly into the sixfold summation (39) the time consumed to evaluate these becomes insurmountable. To circumvent this obstacle we note that many terms in the sums actually depend on very few parameters, the range of these parameters is restricted and the same functional forms repeat themselves. Thus a natural solution is to tabulate these forms and the subsums. In our Coulomb matrix element code we used the

tabulated functions

$$\begin{aligned}
D(i) &= i! \\
F(n, \ell, \kappa) &= \frac{(n + \ell)!}{(n - \kappa)!(\ell + \kappa)!} \\
&= \frac{D(n + \ell)}{D(n - \kappa)D(\ell + \kappa)} \\
G(n, \ell, \kappa) &= \frac{(n + \ell)!}{\kappa!(n - \kappa)!(\ell + \kappa)!} = \frac{F(n + \ell)}{D(\kappa)} \\
H(s) &= \frac{\Gamma(s + \frac{1}{2})}{2^{s+1}} \\
I(q_1, q_2, \ell) &= D(q_1)D(q_2) \sum_{s=0}^{q_1} (-1)^s G(q_1, \ell, s) \\
&\quad \times \sum_{t=0}^{q_2} (-1)^t G(q_2, \ell, t) H(t + s + \ell).
\end{aligned}$$

Now the summations Σ in the expression (39) can be written as

$$\begin{aligned}
\Sigma &= \sum_{\kappa_1=0}^{n_1} (-1)^{\kappa_1} G(n_1, \ell_1, \kappa_1) \sum_{\kappa_2=0}^{n_2} (-1)^{\kappa_2} G(n_2, \ell_2, \kappa_2) \\
&\quad \times \sum_{\kappa_3=0}^{n_3} (-1)^{\kappa_3} G(n_3, \ell_3, \kappa_3) \sum_{\kappa_4=0}^{n_4} (-1)^{\kappa_4} G(n_4, \ell_4, \kappa_4) \\
&\quad \times I(\kappa_1 + \kappa_4 + \frac{1}{2}(\ell_1 + \ell_4 - k), \kappa_2 + \kappa_3 \\
&\quad + \frac{1}{2}(\ell_2 + \ell_3 - k)). \tag{A.1}
\end{aligned}$$

Although the summation here is still fourfold it is nevertheless several orders of magnitude faster than the original one (39) and as such fast enough for our purposes.

Under the influence of the SO coupling the total spin S of our many-electron system is not a conserved quantity. As a consequence of this we cannot fix the total S_z of the many-body basis. This degree of freedom tends to make the number of non-interacting many-body states of the basis very large even for a small number of electrons, and even if the conservation of the total angular momentum $J_z = L + S_z$ is taken into account. For example, to achieve a convergence for a four electron system in the parabolic confinement with harmonic potential ($\hbar\omega_0$) of few meV the size of the basis must be *of the order of a million*. Furthermore, since we want to study properties of the eigenstates, such as polarization and dipole matrix elements between states, we also need the relevant eigenvectors. Clearly the sheer size of the matrix prohibits a full diagonalization and we have to resort to an iterative scheme aimed to search a given number of energetically lowest eigenvectors. Of course the algorithm should be fast and hopefully also robust.

The algorithm proposed by Davidson and Liu (DL) to evaluate the eigenvalues and eigenvectors of “monster

matrices” [50] seem to fit our criteria. Like any other iterative method it transforms the diagonalization of a matrix A to minimization of the Rayleigh quotient

$$\lambda = \frac{x^T A x}{x^T x}, \tag{A.2}$$

where x represents the column vector of the coefficients in the superposition of the basis states. Also, as in many other methods, the only operations involving the matrix A are vector multiplications. This allows us to exploit fully the sparseness of A , i.e. we have to store only the non-zero elements.

The key idea behind practically any iterative method subjecting the matrix only to multiplication is to search the minimum of the quotient (A.2) in a (very small) subspace and to update this subspace in each iteration step. How this updating is performed depends on the method. For example, in the common conjugate gradient method the subspace is two-dimensional and spanned by the gradient g at current position x and a vector s conjugate to it with respect to A (i.e. $s^T A g = 0$).

In the DL method the dimension of the search space varies from step to step. Suppose that at a given step our search space \mathcal{S} is spanned by the orthonormal vectors s_1, \dots, s_K (the dimension K must, of course, be greater than the number of required eigenstates). Finding the minimum of (A.2) in this subspace corresponds to the diagonalization of the $K \times K$ matrix $\mathcal{S}^T A \mathcal{S}$ (we take \mathcal{S} to represent also the matrix with columns s_k). As a result we get K eigenvalues μ_k and K eigenvectors z_k , each of dimension K . The expanded vectors

$$y_k = \sum_{i=1}^K z_{k,i} s_i$$

will approximate the eigenvectors and the quantities μ_k the eigenvalues we are seeking for. The next task in the iteration step is to update the subspace \mathcal{S} . For that purpose we pick up a certain number (a parameter depending for example on the size of the computer memory) of the residuals

$$r_k = (A - \mu_k) y_k$$

with largest norms. The selected residuals are orthonormalized with respect to the space \mathcal{S} and then appended to it. So, in each step the dimension of the search space and the size required to store it increases and we may eventually exhaust all the memory. At this point we compress the space \mathcal{S} to its bare minimum comprising only as many vectors as we are required to find. These vectors are selected from the set $\{y_k\}$ and are the ones with smallest μ_k .

-
- [‡] Electronic mail: tapash@physics.umanitoba.ca
- [1] T. Chakraborty, F Peeters, and U. Sivan (Eds.), *Nano-Physics & Bio-Electronics: A New Odyssey* (Elsevier, 2002).
- [2] P.A. Maksym and T. Chakraborty, Phys. Rev. Lett. **65**, 108 (1990).
- [3] T. Chakraborty, Comments Condens. Matter Phys. **16**, 35 (1992); V. Gudmundsson, A. Manolescu, R. Krahne, and D. Heitmann, in Ref. [1], Ch. 7.
- [4] T. Chakraborty, *Quantum Dots* (North-Holland, Amsterdam, 1999).
- [5] C. Sikorski and U. Merkt, Phys. Rev. Lett. **62**, 2164 (1989).
- [6] See, for example, I. Magnusdottir and V. Gudmundsson, Phys. Rev. B **60**, 16591 (1999); R. Krahne, et al., *ibid.* **63**, 195303 (2001); E. Lipparini, et al. *ibid.* **56**, 12375 (1997); P.A. Maksym, Physica B **184**, 385 (1993); T. Seki, Y. Kuramoto, and T. Nishino, J. Phys. Soc. Jpn. **65**, 3945 (1996); M. Wagner, A.V. Chaplik, and U. Merkt, *ibid.* **51**, 13817 (1995); B. Meurer, D. Heitmann, and K. Ploog, Phys. Rev. Lett. **68**, 1371 (1992); T. Chakraborty, V. Halonen, and P. Pietiläinen, Phys. Rev. B **43**, 14289 (1991).
- [7] D. Mowbray and J. Finley, in Ref. [1], Ch. 3; M.S. Skolnick and D.J. Mowbray, Physica E **21**, 155 (2004).
- [8] A.J. Shields, et al., in Ref. [1], Ch. 4.
- [9] V. Fock, Z. Phys. **47**, 446 (1928); C.G. Darwin, Proc. Cambridge Philos. Soc. **27**, 86 (1930).
- [10] For a similar result in a parabolic quantum well, see, L. Brey, N.F. Johnson, and B.I. Halperin, Phys. Rev. B **40**, 10647 (1989).
- [11] T. Chakraborty and P. Pietiläinen, Phys. Rev. Lett. (2005).
- [12] D.D. Awschalom, D. Loss, and N. Samarth (Eds.), *Semiconductor Spintronics and Quantum Computation* (Springer, 2002); D. Grundler, Phys. World **15**, 39 (2002); S.A. Wolf, et al., Science **294**, 1488 (2001); G.A. Prinz, Phys. Today **48**, 58 (1995).
- [13] *Proceedings of the First International Conference on the Physics and Applications of Spin Related Phenomena in Semiconductors*, edited by H. Ohno [Physica E **10** (2001)]; G. Schmidt, C. Gould, and L.W. Molenkamp, Physica E **25**, 150 (2004).
- [14] W.H. Kuan, C.S. Tang, W. Xu, J. Appl. Phys. **95**, 6368 (2004).
- [15] O. Voskoboynikov, C.P. Lee, and O. Tretyak, Phys. Rev. B **63**, 165306 (2001).
- [16] O. Voskoboynikov, O. Bauga, C.P. Lee, and O. Tretyak, J. Appl. Phys. **94**, 5891 (2003).
- [17] M. Governale, Phys. Rev. Lett. **89**, 206802 (2002).
- [18] J.H. Creemers, P.W. Brouwer, and V.I. Falko, Phys. Rev. B **68**, 125329 (2003).
- [19] H. Tütüncüler, R. Koc, and E. Olgar, J. Phys. A **37**, 11431 (2004).
- [20] E. Tsitsishvili, G.S. Lozano, and A.O. Gogolin, Phys. Rev. B **70**, 115316 (2004).
- [21] M. Valin-Rodriguez, Phys. Rev. B **70**, 033306 (2004).
- [22] M. Valin-Rodriguez, A. Puente, and L. Serra, Phys. Rev. B **69**, 153308 (2004).
- [23] M. Valin-Rodriguez, A. Puente, and L. Serra, Phys. Rev. B **69**, 085306 (2004).
- [24] M. Valin-Rodriguez, A. Puente, and L. Serra, Phys. Rev. B **66**, 165302 (2002).
- [25] P. Lucignano, B. Jouault, A. Tagliacozzo, and B.L. Altshuler, Phys. Rev. B **71**, 121310 (2005); P. Lucignano, B. Jouault, and A. Tagliacozzo, *ibid.* **69**, 045314 (2004).
- [26] C.F. Destefani, S.E. Ulloa, and G.E. Marques, Phys. Rev. B **69**, 125302 (2004); **70**, 205315 (2004).
- [27] S. Debald and C. Emary, Phys. Rev. Lett. **94**, 226803 (2005).
- [28] J. Königmann, R.J. Haug, D.K. Maude, V.I. Falko, and B.L. Altshuler, Phys. Rev. Lett. **94**, 226404 (2005).
- [29] S. Bellucci and P. Onorato, Phys. Rev. B **72**, 045345 (2005).
- [30] J. Fransson, et al., Phys. Rev. B **67**, 205310 (2003).
- [31] T. Chakraborty and P. Pietiläinen, Phys. Rev. B **71**, 113305 (2005).
- [32] M.A. Eriksson, et al., Quantum Information Processing **3**, 133 (2004); D. Loss, G. Burkard, and D.P. DiVincenzo, J. Nanoparticle Res. **2**, 401 (2000); R. Hanson et al., Phys. Rev. Lett. **94**, 196802 (2005); D. Stepanenko and N.E. Bonesteel, Phys. Rev. Lett. **93**, 140501 (2004).
- [33] S. Bandyopadhyay, Phys. Rev. B **61**, 13813 (2000).
- [34] D. Grundler, Phys. Rev. Lett. **84**, 6074 (2000); C.-M. Hu, J. Nitta, T. Akazaki, H. Takayanagi, J. Osaka, P. Pfeffer and W. Zawadzki, Physica E **6**, 767 (2000); C.-M. Hu, et al., Phys. Rev. B **60**, 7736 (1999); Y. Sato, T. Kita, S. Gozu, and S. Yamada, J. Appl. Phys. **89**, 8017 (2001); J. Nitta, T. Akazaki, and H. Takayanagi, Phys. Rev. Lett. **78**, 1335 (1997).
- [35] Y.A. Bychkov and E.I. Rashba, J. Phys. C **17**, 6039 (1984).
- [36] H.A. Bethe and E.E. Salpeter, *Quantum Mechanics of One- and Two-Electrons Atoms* (Springer, Berlin, 1957).
- [37] W. Zawadzki and P. Pfeffer, Semicond. Sci. Technol. **19**, R1 (2004).
- [38] R.J. Haug, J. Weis, R.H. Blick, K von Klitzing, K. Eberl, and K. Ploog, Nanotechnology **7**, 381 (1996); T Schmidt, R.J. Haug, K. von Klitzing, A. Förster, and H. Lüth, Phys. Rev. Lett. **78**, 1544 (1997).
- [39] R.C. Ashoori, et al., Phys. Rev. Lett. **71**, 613 (1993).
- [40] V. Halonen, P. Pietiläinen, and T. Chakraborty, Europhys. Lett. **33**, 377 (1996).
- [41] P. Tonello and E. Lipparini, Phys. Rev. B **70**, 081201 (2004).
- [42] G.A. Khodaparast, R.E. Doezema, S.J. Chung, K.J. Goldammer, and M.B. Santos, Phys. Rev. B **70**, 155322 (2004).
- [43] B. Jouault, G. Santoro, and A. Tagliacozzo, Phys. Rev. B **61**, 10242 (2000).
- [44] D.G. Austing, et al., in Ref. [1], Ch. 2.
- [45] T. Chakraborty, V. Halonen, and P. Pietiläinen, Phys. Rev. B **43**, 14289 (1991); A. Wensauer, O. Steffens, M. Suhrke, and U. Rössler, *ibid.* **62**, 2605 (2000); J. Kolehmainen, S.M. Reimann, M. Koskinen, and M. Manninen, Eur. Phys. J. B **13**, 731 (2000); A. Harju, S. Siljamäki, and R.M. Nieminen, Phys. Rev. Lett. **88**, 226804 (2002); Z. Dai, et al., Eur. Phys. J. B **29**, 141 (2002); Appl. Phys. Lett. **80**, 2577 (2002); A.J. Markvoort, P.A.J. Hilbers, and R. Pino, J. Phys.: Condens. Matter **15**, 6977 (2003); B. Szafran, F.M. Peeters, and S. Bednarek, Phys. Rev. B **70**, 205318 (2004); T. Hatano,

- et al., Phys. Rev. Lett. **93**, 066806 (2004); L.-X. Zhang, et al., Phys. Rev. B **69**, 245301 (2004); B. Szafran and F.M. Peeters, *ibid.* **71**, 245314 (2005).
- [46] J.J. Palacios and P. Hawrylak, Phys. Rev. B **51**, 1769 (1995); J.H. Oh, K.J. Chang, G. Ihm, and S.J. Lee, *ibid.* **53**, 13264 (1996); W.-Y. Ruan and H.-F. Cheung, Eur. Phys. J. B **3**, 407 (1998); H. Imamura, P.A. Maksym, and H. Aoki, Phys. Rev. B **53**, 12613 (1996); **59**, 5817 (1999); Y. Tokura, D.G. Austing, and S. Tarucha, J. Phys.: Condens. Matter **11**, 6023 (1999); B. Partoens, A. Matulis, and F.M. Peeters, Phys. Rev. B **59**, 1617 (1999); G. Burkard, G. Seelig, and D. Loss, *ibid.* **62**, 2581 (2000); B. Partoens and F.M. Peeters, Europhys. Lett. **56**, 86 (2001); W. Xie and P. Sun, J. Phys.: Condens. Matter **14**, 7245 (2002); S. Bednarek, T. Chwiej, J. Adamowski, and B. Szafran, Phys. Rev. B **67**, 205316 (2003); D. Bellucci, et al., *ibid.* **69**, 201308 (2004); M. Rontani, et al., *ibid.* **69**, 085327 (2004); G. Ortner, et al., Phys. Rev. Lett. **94**, 157401 (2005); D. Bellucci, F. Troiani, G. Goldoni, and E. Molinari, J. Lumin. **112**, 109 (2005).
- [47] X.-Q. Li and Y. Arakawa, Phys. Rev. A **63**, 012302 (2000); J.M. Elzerman, et al., Phys. Rev. B **67**, 161308 (2003); X.-Q. Li and Y. Yan, *ibid.* **65**, 205301 (2002); H. Qin, et al., *ibid.* **64**, 241302 (2001); T. Hayashi, et al., Phys. Rev. Lett. **91**, 226804 (2003); S. Vorozhitsov, E.R. Mucciolo, and H.U. Baranger, Phys. Rev. B **69**, 115329 (2004); J. Gorman, D.G. Hasko, and D.A. Williams, Phys. Rev. Lett. **95**, 090502 (2005).
- [48] H. Sasakura, et al., Semicond. Sci. Technol. **19**, S409 (2004).
- [49] M. Stone, H.W. Wyld, and R.L. Schult, Phys. Rev. B **45**, 14156 (1992).
- [50] E.R. Davidson, Computers in Physics **7**, 519 (1993).